Switching Notes
Note 3
August 1964

Investigation of a Laser Triggered Spark Gap

Lt Winston K. Pendleton
Air Force Institute of Technology
and
Air Force Weapons Laboratory

Abstract

A focused, Q-spoiled laser beam was used to produce an arc in a sphere-sphere electrical gap charged to within 30-90% of self breakdown. The time response of the triggering was measured as a function of: laser beam power, 0-80 megawatts; fill gas, SF_6, N_2, Air; gas pressure, 100-1400 mm of Hg; electrode spacing, .4-1.5 cm; gap electric field, 10-100 KV/cm and focus point location. Short delay times as low as 20 ns were measured in SF_6 at atmospheric pressure. Generally delay times varied inversely with the electric field, gas pressure and focus point distance from the anode surface. The results obtained were considered consistent with those predicted by the streamer theory of arc formation.

Preface

The initial purpose for this report is to serve as the written thesis fulfilling the requirements for the Masters' Degree in Nuclear Engineering from the Air Force Institute of Technology. It is sincerely hoped, however, that it will be a worthwhile contribution to the scientific literature as the first work concerning laser spark gap triggering and that its contents will be discussed and amplified in the search for better understanding of the phenomenon.

I would like to give thanks to all the people who helped me in this study. By far the most gratitude must go to Dr. Arthur H. Guenther for conceiving and demonstrating the laser triggering idea. His unending experimental ingenuity, patience and inspiration not only made my stay at Kirtland Air Force Base delightful, but improved immeasurably the quality of the work. In addition, I would like to acknowledge the help of: Lt. Charles W. Bruce and Lt. P.V. Avizonis for their assistance with the laser aspect of the study; T/Sgt Vincent C. Henrick and Leroy A. Johns whose photographic skills and reproduction support are liberally displayed in the body of this report; A1C Mel K. Pfeffer for electronics and oscilloscope assistance; A3C Antonio C. Regel, drafting and graphic drawings; S/Sgt Travis E. McClarney, head of the machine shop, for speedy, high quality

work; and the general technicians who offered their experience, companionship and encouragement: Albert B. Griffin, F. Oliver Westfall, A2C Robert D. Goligowski and A1C Willy E. Kunzler. Thanks also go to Dr. William Lehmann for a critical review of the paper and to my fiance, Judy McCutcheon, for correcting my grammatical errors and typing the manuscript.

Finally, I would like to say that I accept the responsibility for the contents or lack of contents of this report, especially in the sections concerning theory and conclusions. It is hoped that future work will be more enlightening.

WKP

Contents

Contents

List of Symbols

E_L - Laser beam energy (joules)

$\bar{E}_L$ - Laser beam electric field vector

Δt_L - Laser pulse width at half maximum (nanoseconds)

d - Axial distance between electrode surfaces (cm)

d_n - Distance between laser beam focus point and cathode (-) sphere (cm)

V_g - Potential between electrodes (kilovolts)

V_{SB} - Self breakdown voltage of gap (KV)

V_T - Lowest voltage for which gap triggerable (KV)

E_g - Electric field strength between spheres (volts/cm)

p - Gas pressure in the gap (mm of Hg)

Δt_D - Time delay between laser pulse arrival at gap and current flow (ns)

α - First Townsend coefficient

List of Figures

List of Figures

INVESTIGATION OF A LASER TRIGGERED SPARK GAP

I. Introduction

Statement of Problem

In July, 1963, it was demonstrated by Dr. Arthur H. Guenther and Albert B. Griffin of the Air Force Weapons Laboratory (AFWL), Kirtland Air Force Base, that a sphere-sphere electrical spark gap charged to within one kilovolt of self breakdown could be triggered by a Q-spoiled ruby laser. It was immediately realized that a detailed, careful investigation of this phenomenon should be undertaken to determine the behavior of this device and ultimately lead to a theoretical understanding of the laser beam-gap interaction. It was the purpose of this research effort to design and implement an experimental study which would produce meaningful data pertinent to the laser beam-gap triggering interaction and see if the results were consistent with an existing arc formation theory. The natural outgrowth of this work would be the establishment of measuring techniques, realization of the important parameters of the system, formulation of possible applications and limitations of the device and finally, to serve as a foundation for further study.

Importance of Problem

The triggering of a spark gap by a laser was conceived as a switching device to meet the requirements of a high voltage, high energy storage device being considered by AFWL in connection with a Radio Corporation of America (RCA) contract. The proposed storage system would hold about 500,000 joules of electrical energy at 10 million volts and discharge into a transducer (wire, foil or field emission assembly), thus being transformed into thermal, electromagnetic and mechanical energy. This energy would then be used for weapon simulation, radiation effects investigation and high temperature plasma studies. The characteristics of the switch considered most important were that it 1) carry at least one million amperes with 2) very low inductance, 3) have a long lifetime with minimum maintenance, 4) have a switching delay less than 5 nanoseconds with 5) jitter less than 1 nanosecond and 6) be simple and inherently safe to operate. No existing high voltage switching device at the time was felt properly suited to meet these requirements. It was believed and subsequently shown that a laser triggered switch has a high probability of meeting these requirements. The factor of safety is its most outstanding feature since there is no electrical connection between the storage system and the triggering device. The results obtained from the studies covered by this paper also indicate that the delay, jitter and lifetime requirements might be readily achieved.

Survey of Previous Study

The only two experimental or theoretical studies of spark gap triggering by lasers known to the author are those conducted at AFWL from 11 July 1963 - 25 July 1963 and the continuation of the project from 1 Oct 64 - 20 March 1964 which is covered by this paper. The initial studies in July 63 were primarily of a phenomenological nature to see if the triggering phenomenon would occur in different gases and obtain some indications of the time delays to be expected. The study also pointed out some of the major problems associated with this experiment. The second attempt on the experiment was intended to be more conclusive and show a systematic approach to the gathering of data. Primarily this involved refinements in alignment procedure, scope triggering and delay measurements. Additional difficulties were encountered; solutions are suggested at the end of the report.

Organization of Paper

The body of this paper will contain five main sections. Section II will present a brief outline of the existing theory of gaseous conduction, particularly that dealing with the arc discharge. The mechanisms believed to be responsible for the initial arc formation will be discussed. In order to shed some light on the laser influence in the gap, a brief discussion of the optical ionization in air is included. The theory section of this paper is presented as background material to aid the reader in evaluating the results. Only semiquantitative comparisons are made between the theory and results

obtained. Section III explains the experimental design. It includes a discussion of the parameters to be varied, a description of the two lasers and spark gap chambers, and an explanation of the diagnostic techniques for monitoring the laser beam and spark gap switching. Section IV contains the data and results. Only representative raw data is included in this section. It ends with an analysis and estimate of the errors present in the various measured parameters. The discussion and conclusions resulting from this experimental study are presented in Section V. Ideas concerning mechanisms and models are discussed here. The final section (Section VI) gives recommendations for further study. Possible solutions to existing problems are presented and pertinent data not obtained here is suggested. No recommendations for final design of the operational switch are made but ways of improving the delay and jitter are briefly mentioned.

Two appendices follow the body. Alignment, calibration and other experimental procedures are fully described in Appendix A. Appendix B contains additional graphs to give a more complete presentation of the results obtained.

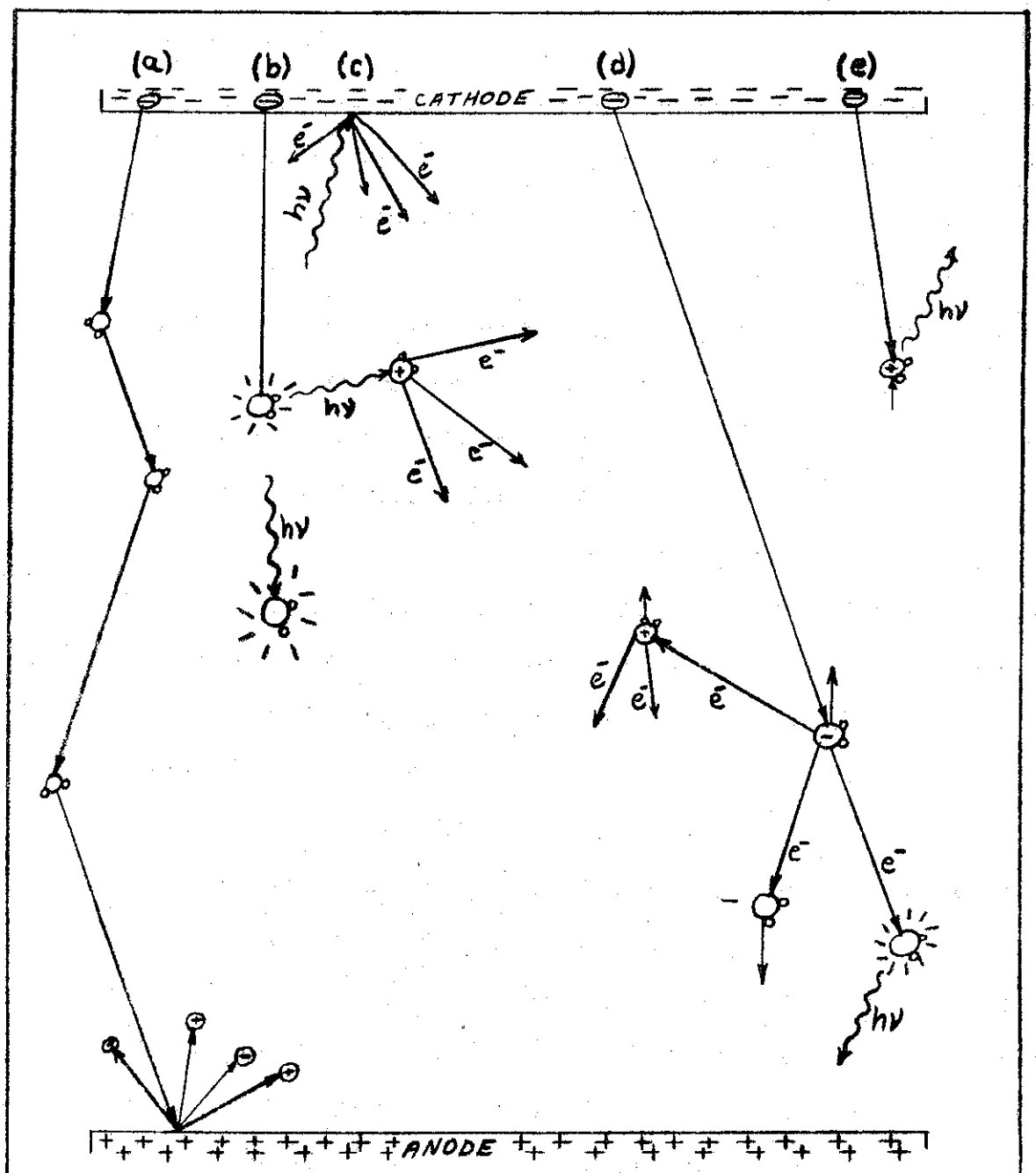

Fig. 1 Gaseous Conduction Processes

II. Theory

The major effort associated with this investigation was in designing and implementing the experiments to obtain the interaction data. Thorough analysis and interpretation of the results was not accomplished. For this reason, this section on theory is presented in a qualitative manner as background material and should not be taken as a conclusive explanation of the results obtained.

The theory of electrical descharges in gases is still a widely discussed question. There is good reason for this. Unlike a metal, where the electron energies are seriously restricted in the lattice, a gaseous medium provides a much wider range of possible energies. Thus a greater number of processes are in operation prior to and during an electrical discharge. This is especially true of the arc discharge observed at the higher electric field strengths. Figure 1 is a schematic diagram showing the processes and interconnections between processes associated with such a discharge between two electrodes. The upper electrode is the cathode, the electrons tend to move against the field toward the anode. Path (a) shows an electron making elastic collisions with the gas molecules in the gap. This is by far the most common occurrence since relatively few electrons ever achieve sufficient energy to excite or ionize the gas (Ref 7:3). When an electron reaches the anode it may simply be absorbed or it may inject charged carriers into the gap. Path (b) might be followed by an electron which has sufficient energy to excite a gas molecule. The result might be deexcitation by nonradiative collisions or the

emission of a photon with energy hν. This photon is then free to ionize, excite or decompose neighboring molecules or even initiate photoelectric emission as at point (c). An electron such as (d) might gain enough energy to ionize directly, thus forming a positive ion and one or more free electrons. The positive ions formed are accelerated toward the cathode. A free electron may also attach itself to a molecule and form a negative ion. As for electron (e) there can be recombination with positive ions forming a characteristic photon. For mixtures of gases, like air, additional interactions are present involving metastable states. With all these interactions occurring simultaneously, it is with good reason that no simplified theory of gaseous discharge has been adopted. Two arc discharge models do exist which give reasonably good predictions of arc formation. These are the Townsend avalanche theory and the streamer theory. It is generally accepted that the Townsend theory should be used at low values of pd (pressure x electrode spacing) and that the streamer theory is more correct at higher pd values. The crossover point is somewhere near a value of pd = 200 cm x mm of Hg. (Ref 6:27). Initially, a theory was sought which would successfully predict the self breakdown voltage of a gap; but, lately the emphasis has been on explaining the formative time lags of the arc (Ref 3:109). This was the approach taken in this study. Based on the results of this investigation it is the opinion of the author that the streamer theory is more satisfactory in explaining the short delay times observed (10^{-8} - 10^{-7} seconds). A brief discussion of its main features is now presented.

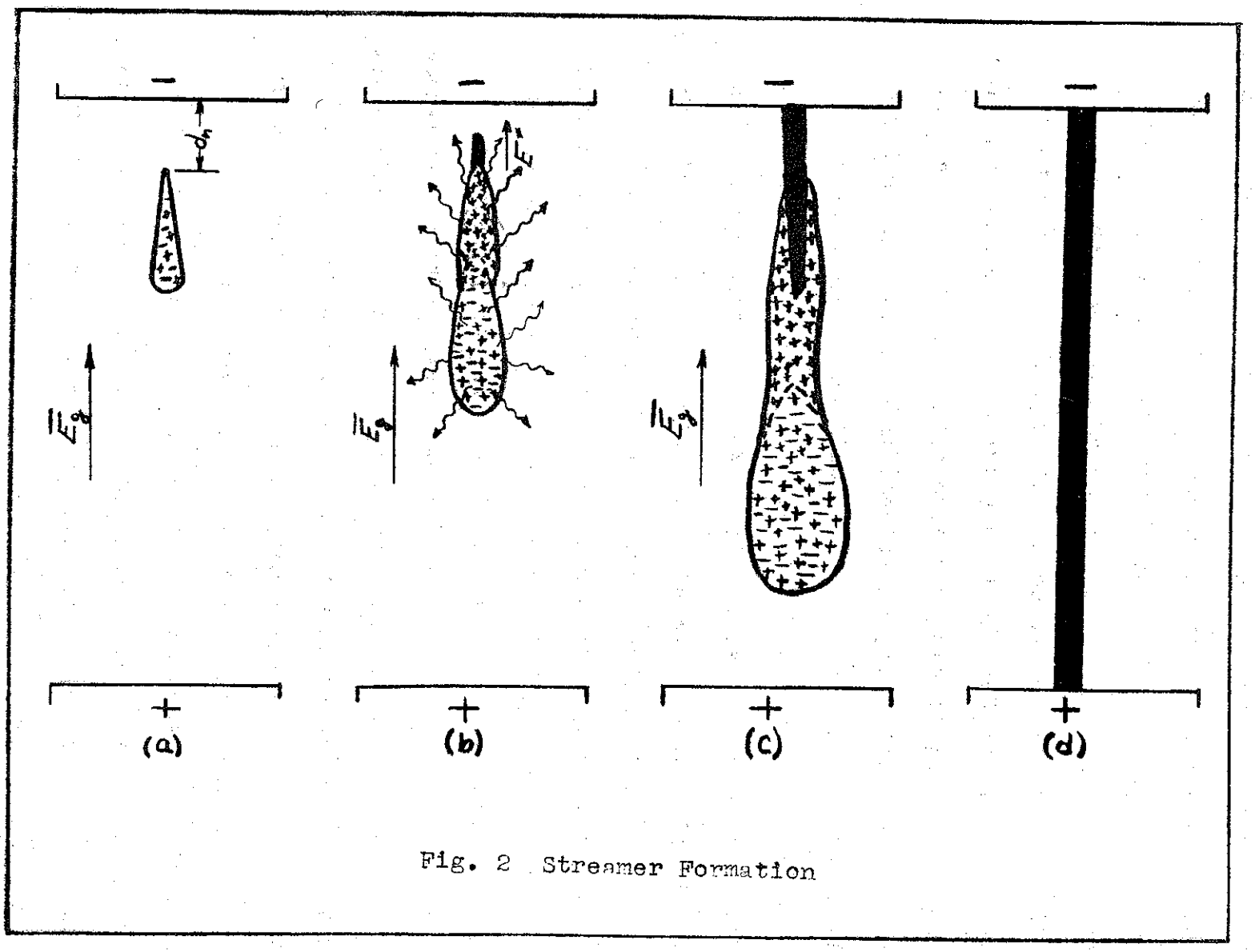

Fig. 2 Streamer Formation

Streamer Theory

The streamer theory of arc discharge formation was postulated as an explanation for the very rapid arc formation times encountered at highly overvoltaged gaps. Whereas the Townsend theory stressed the importance of positive ions emitted from the anode, the new theory sought a source of charge carriers propagating much faster than the ions or electrons in the gap. The streamer theory is based on the photoionization of the gas by photons emitted from excited molecules in the positive space charge cloud resulting from a Townsend type avalanche.

Figure 2 gives a time resolved diagram of streamer development. Frame (a) of the process shows the initial Townsend avalanche formed when an electron or clump of electrons starting at d_n centimeters from the cathode is accelerated toward the anode. The population of ions and electrons increases at the rate $d^{\alpha x}$, where α, the first Townsend coefficient, is the number of new electrons produced per electron per centimeter. The two charged regions diffuse apart under the influence of the gap electric field. Since the bulkier positive ions diffuse more slowly, they remain in a compact cloud near their creation point, while the electron avalanche continues to grow. Assuming a nearly spherical volume of positive charges the space charge field, $\bar{E}^+$, can be calculated. It enhances the DC field between the positive cloud and the cathode by as much as 20% (Ref 6:37). Within the positive cloud are from four to ten times as many excited atoms and molecules as ions giving off photons in all directions. These photons are absorbed in the

neighboring neutral gas resulting in further ionization. Many of the resulting electrons will lie in the enhanced field region where α is largest and be drawn into the positive cloud. The positive ions they leave behind have the effect of rapidly propagating the positive space charge region toward the cathode. This self propagating space charge streamer is shown in Fig. 2b. Some believe that the same process occurs at the avalanche tip (Ref 7:181-183) but this concept is not as easily justified due to the lack of a net space charge region there. At any rate, once the positive streamer reaches the cathode (c), the DC potential wave propagates down the conducting streamer toward the anode, thus forming a complete conducting bridge or arc across the gap, Fig. 2d.

The velocities of propagation of the various regions have been measured. The initial avalanche velocity is about 2×10^7 cm/sec, the streamer velocity toward the cathode is about 1.3×10^8 cm/sec, and the potential wave propagation can be as high as 10^9 cm/sec, (Ref 6:39,40). A positive ion cloud would propagate at approximately 2×10^4 cm/sec due to the 10^3 mass factor over electrons (Ref 6:34).

Laser Beam Ionization

According to the streamer theory the arc formation is initiated by an electron or clump of electrons in a Townsend avalanche which gains such proportions that a positive space charge streamer can develop. In the case of an overvoltaged gap it takes only one elctron to trigger the process (Ref 6:26).

Under the conditions of this investigation all triggering was done in undervoltaged gaps, therefore, the initiating process must be viewed in terms of the laser beam interactions with the gas or with the electrodes. The primary interaction is probably the ionization or photoelectric emission of electrons. Both processes have been demonstrated experimentally (Ref 4:342, Ref 2:1-5). Since the photon energy of ruby laser light is 1.78 ev, below the ionization potentials of the inert gases and work functions of the common electrode metals, multiple photon absorptions seem necessary. The high photon densities of a focused laser beam make such interactions highly probable (Ref 9:2229). The ability of multiple photon effects to account for the large number of ion pairs produced has been questioned and a theory of inverse Bremsstrahlung absorption by free electrons and subsequent ionizations has been proposed. It has been calculated that the upper limit for a 30 megawatt laser beam is the production of 10^{16} ion pairs (Ref 8:5).

No theory has yet been offered which accurately accounts for the observed ion production in gases. It seems more fruitful to consider the measured values and their possible relationship to the streamer formation process.

At least two experimental studies have been conducted to measure electron production by a focused laser beam. In one the ionization of a gas was produced between two needle probes to collect the charge formed. The energy of the beam was about 1.5 joules and the measured photoionization was about 10^{8} ion pairs. A comparable number of ions were observed for

conventional laser pulses as for Q-spoiled pulses, thus showing ionization to be more energy dependent than power dependent. The logarithm of the photoionization was linear with laser energy and corresponded to a sixth-power relationship (Ref 2).

The other experimental study of interest concerned photoelectric emission of electrons by a laser beam focused on a metal target. A rough calculation on the data obtained gives a net emission of about 10^{14} electrons. This corresponds to a current density of about 100 A/cm^2 (Ref 4:343).

A considerable amount of research needs to be done before any firm understanding of the ionization process is obtained. Development of diagnostic techniques to yield reliable data are also needed. The problems of laser ionization studies are discussed very well in Reference 10.

III. Experimental Design

Parameters

From the previous section the conclusion is obvious that arc formation and the laser beam-gas interaction are very complex processes and depend on a variety ofparameters. Since the proposed experimental study of laser triggering was being conducted for the first time, it was decided that no system parameters would be excluded from consideration. This then required an experimental set-up and procedure which would specify the condition of the system on each shot and provide for a systematic variation of these parameters. Definition of these variables necessarily preceeded experimental design.

The laser beam was characterized by its energy, average power, polarization and power density at the focus point. Since the laser output could not be predetermined it was necessary to provide a monitoring device capable of measuring the energy and pulse width for each shot. The polarity could be set and power density calculated knowing the focal length of the lens. The other parameters are directly connected with the spark gap chamber. These variables were: diameter and material of the spherical electrodes, perpendicular distance between electrodes at closest approach, location of laser focus with respect to the electrodes, type of gas and gas pressure, gas condition (neutral or partially ionized) and finally the DC potential between the electrodes. These variables represent the state of the system before each experimental shot.

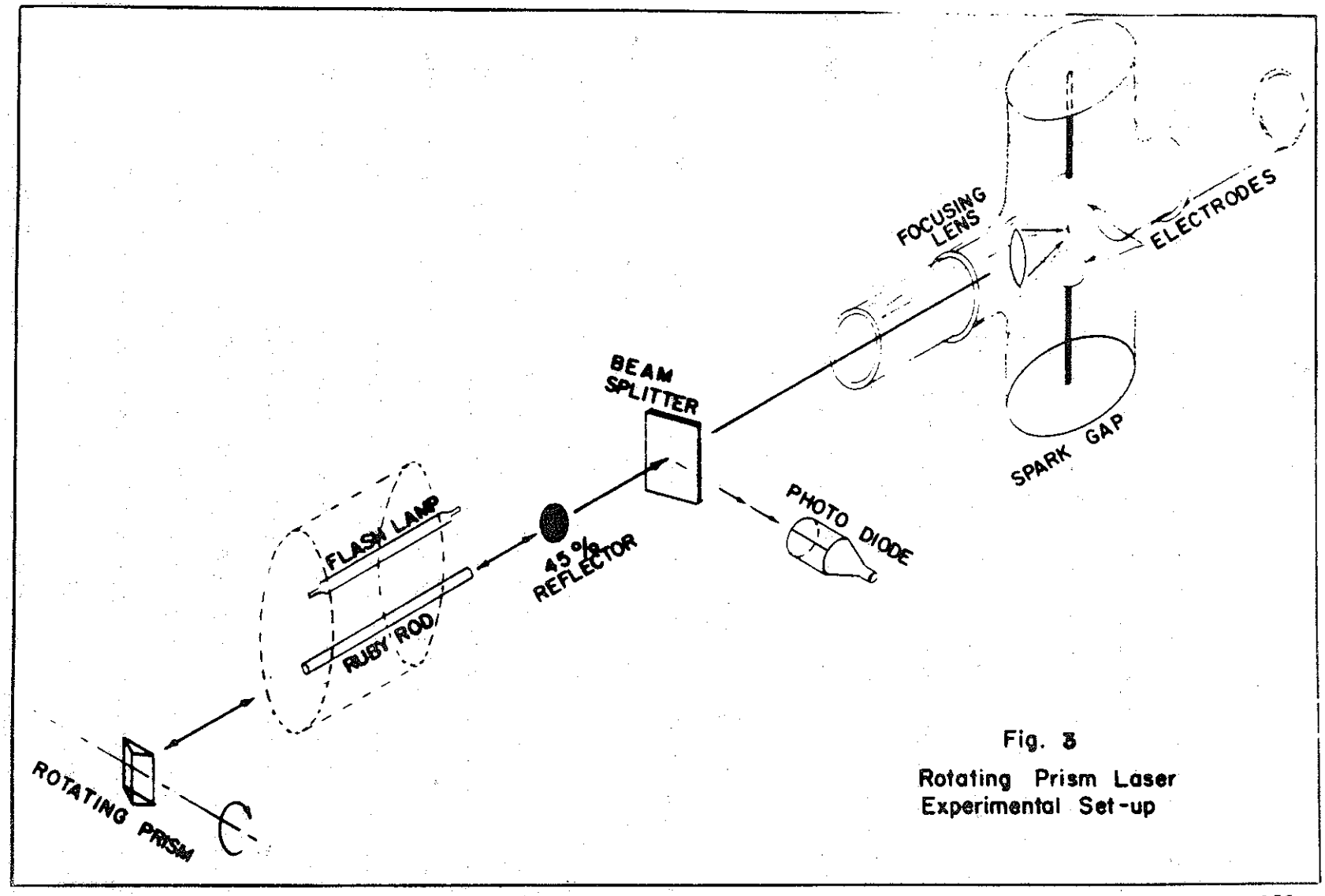

Fig. 8
Rotating Prism Laser
Experimental Set-up

In addition, the time delay between laser pulse arrival at the focus point and the start of current flow in the gap was measured to provide an indication of the laser beam-gap interaction.

Apparatus

Control of the above parameters requires a close interplay of mechanical, electrical and radiative equipment in the actual experiment to perform the necessary measurements. The description of the experimental apparatus is given in this section and is divided into three parts: Laser Systems, Spark Gap Chambers and Control-Diagnostic Equipment.

Laser Systems. Figure 3 shows the essential features of set-up employing the rotating prism laser and the vacuum spark gap chamber. The laser consisted of a commercial Raytheon elliptical reflector head modified to hold a $\frac{1}{2}$ in. diameter by 6 in. long ruby rod with anti-reflective, flat ends. At one focal axis of the elliptic cylinder was mounted an FX 47 flash tube; the ruby rod was at the other focus. The entire head was mounted on two micropositioners which were then mounted to a standard 4 in. optical bench. The rotating prism Q-spoiler was the Bechman and Whitney Corporation model 401 and included the necessary control equipment, model 321, for proper operation of the laser. It was attached to the bench on axis with the ruby rod. On the opposite end of the rod was located a 45% reflective mirror. The prism and mirror constitute the laser resonance cavity. The rotating prism Q-spoiler

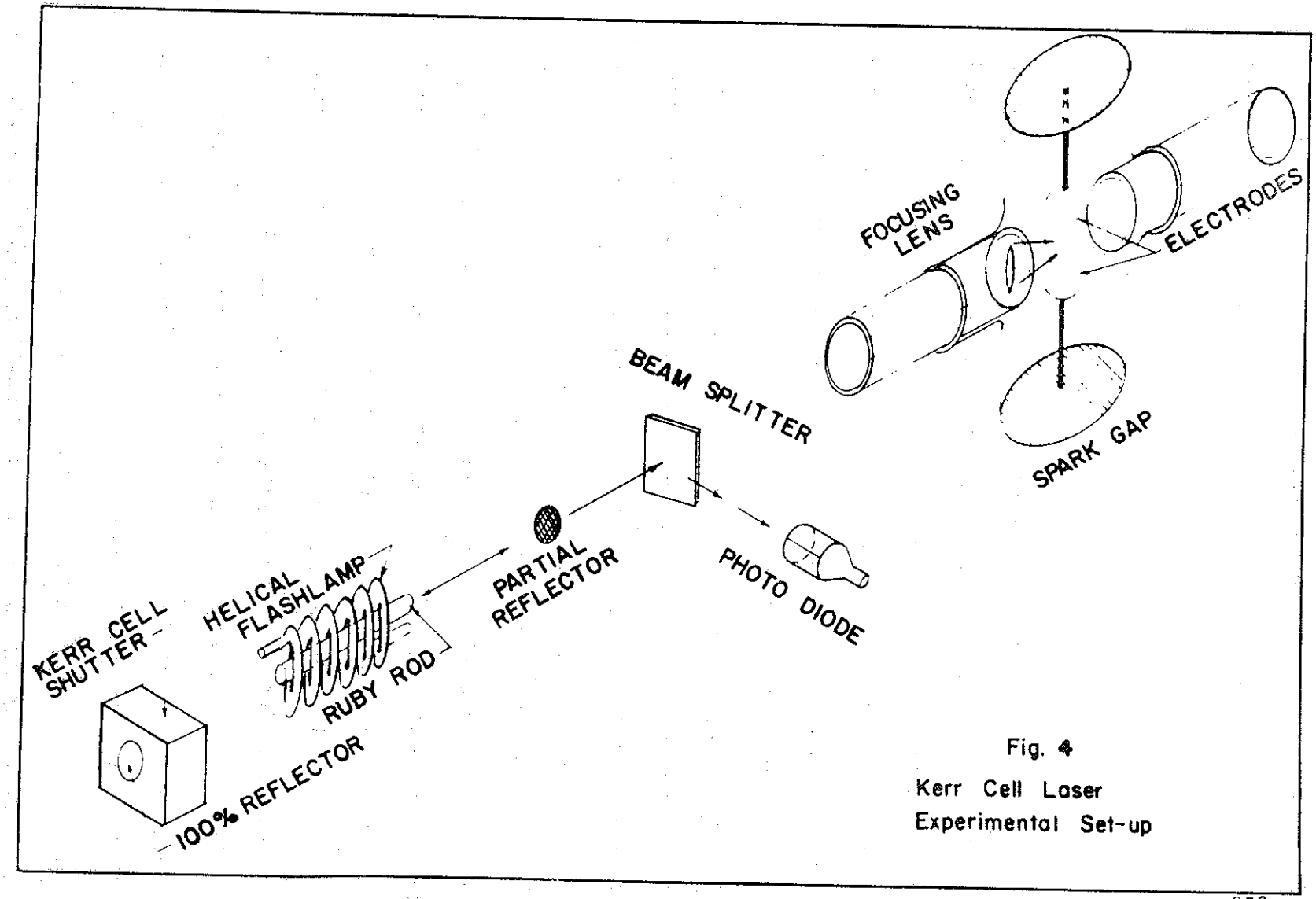

Fig. 4
Kerr Cell Laser
Experimental Set-up

works on the principle that the reflecting surface of the prism becomes perpendicular to the ruby rod at the instant the rod reaches its maximum excitation or population inversion by the pump light. The prism rotates from a position of no optical feedback to one with feedback. The sudden change into a resonance condition is termed Q-spoiling. For proper operation it was necessary to determine the optimum phase relationship between pump light and turbine angle. The experimental procedure for establishing the maximum energy output for any turbine speed is described in Appendix A.

This experimental arrangement was used during most of the study until a more powerful laser became available. The output of the rotating prism was variable from 0-.75 joules with a pulse width at half maximum of from 50-100 nanoseconds (1 ns = 10^{-9} sec.) Thus, the power output varied from 0-15 megawatts. Average power is given by the relation: $\text{Power} = \frac{\text{Energy Out}}{\text{Pulse Width}}$.

Figure 4 shows a similar arrangement with the Kerr cell switched laser used during the last month of the project. The entire unit was a Korad Corporation device consisting of a helical flashlamp surrounding a 3/8 in. diameter by 4 in. long ruby rod. Mounted at one end of the rod was a partial reflector. At the other end was located a 100% mirror and a nitrobenzine filled Kerr cell light shutter for Q-switching. When a high electric field is impressed upon nitrobenzene it becomes a $\frac{1}{4}$ wave light rotator and prevents feedback of the ruby light. At the appropriate time in the pumping process, the field is

removed and a sudden change in the feedback occurs. The output of this unit was measured to be about .8 joule maximum with a pulse width of about 10 ns. The useful range of power values was from 40-80 megawatts.

Spark Gap Chambers. The environmental spark gap chambers into which the laser was focused were of two types. Both consisted of two spherical electrodes mounted on threaded shafts for adjusting gap spacing, gas evacuation and filling outlets, lens holders, observation windows and high voltage connectors. The basic difference between the two was that one was glass, designed for pressures less than two atmospheres absolute and the other was metal, to be used from one atmosphere up to 20 atmospheres.

The glass chamber was a standard 3 in. - 6 in. flanged Kimax Pipe complete with gaskets and fittings. Figure 5 shows the chamber proper without high voltage leads or gas connectors. The modifications included the two lucite lens holders, the spheres and drill rod shafts and the exhaust hole and nipple out the top. The lens holders were designed for 52 mm diameter lens and could be used with 30 mm to about 300 mm focal length lens. In the experiments made during the study only a 52 mm focal length lens was used. The two sphere electrodes were stainless steel, $2\frac{1}{2}$ in. in diameter. With this size sphere the maximum spacing attainable between them was about three centimeters. The diameter of the drill rod shafts was $\frac{1}{2}$ inch. This gives a sphere to shaft diameter ration of 5:1, making the

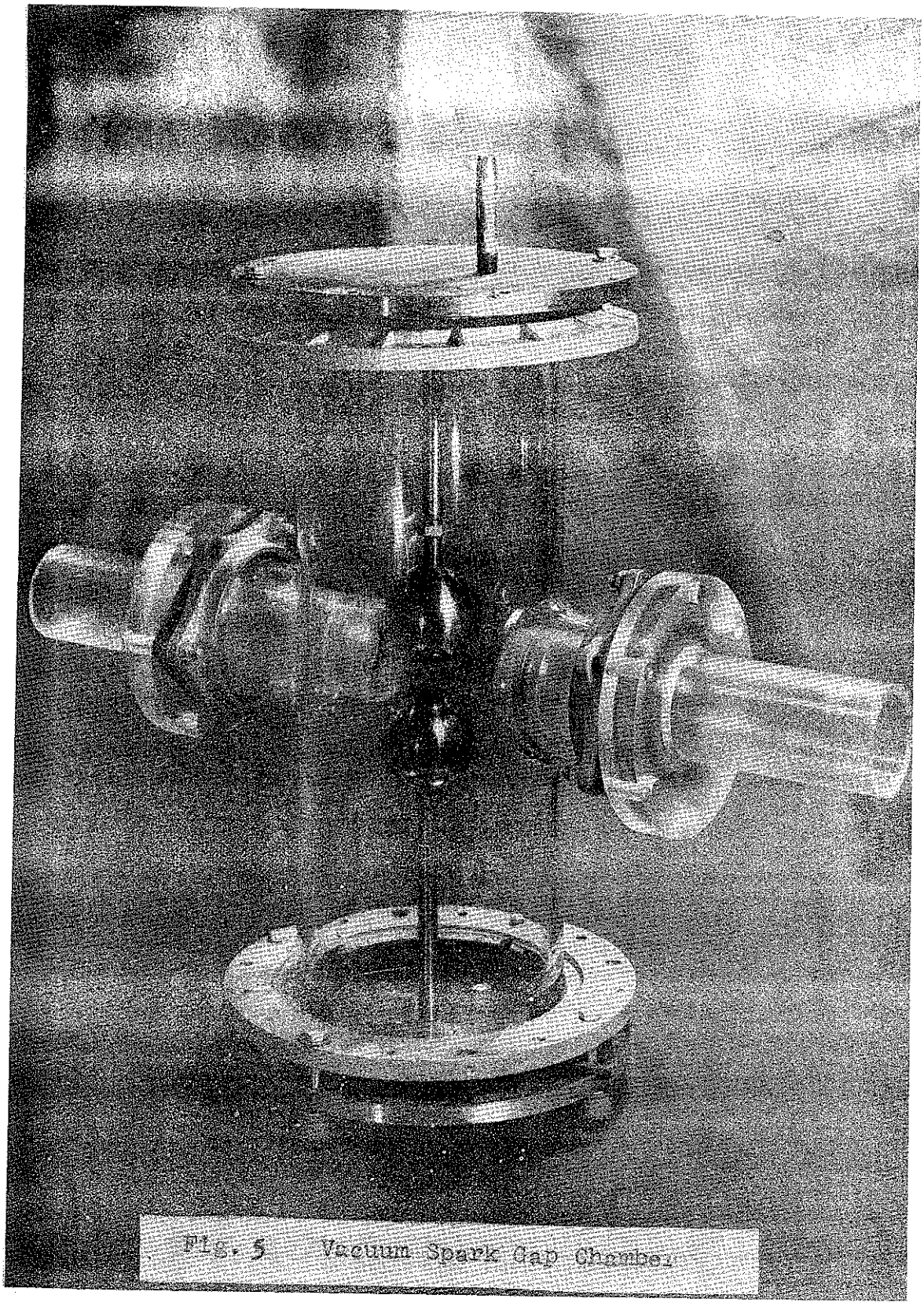

Fig. 5 Vacuum Spark Gap Chamber

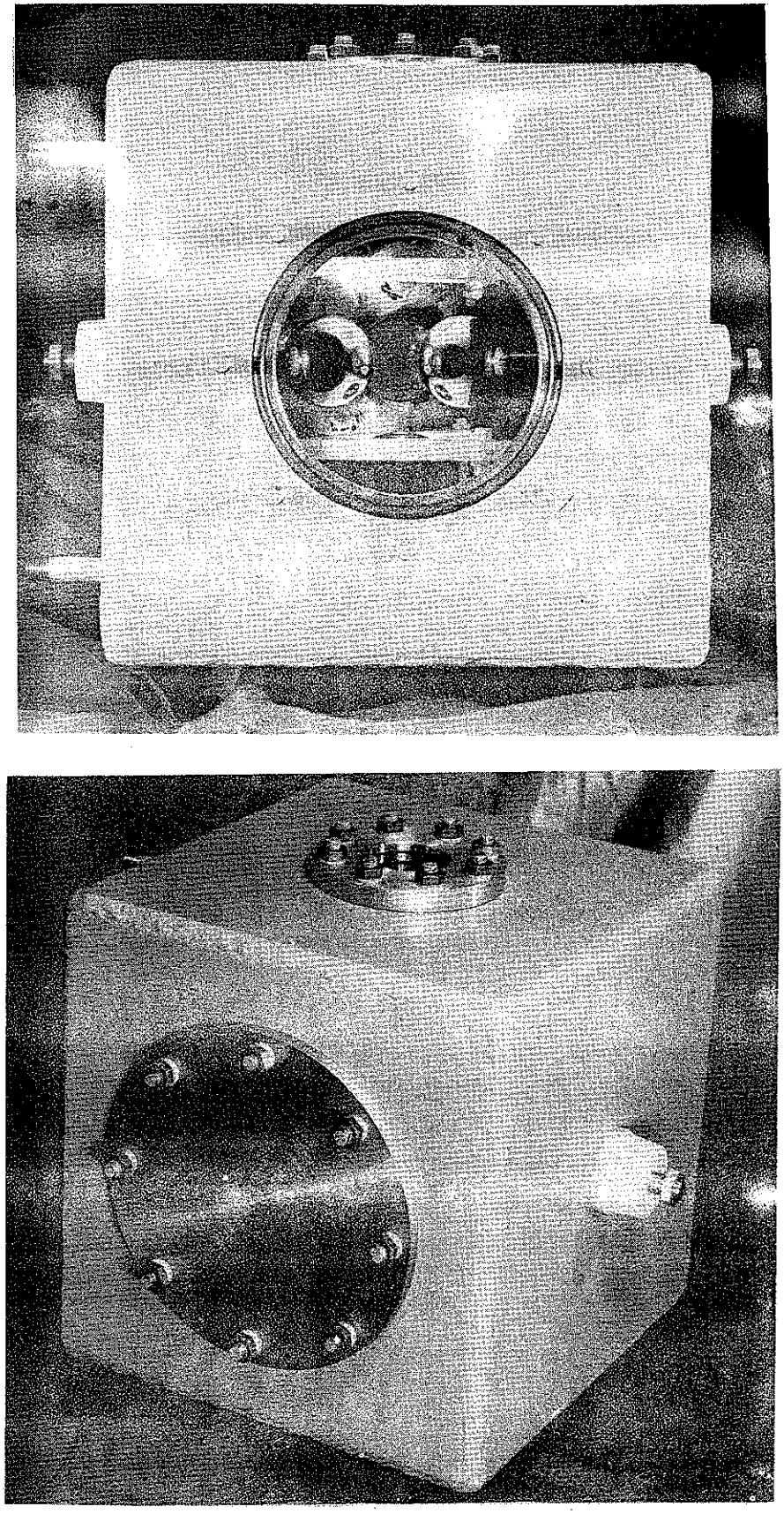

Fig. 6 Pressure Spark Gap Chamber

field very uniform between the electrodes for gap spacings less than 2 cm. Observation of the gap perpendicular to the lens holders gave a relatively undistorted view of the spacing. High voltage and ground connections were attached by 3/8 in. bolts to the top and bottom plates of the chamber. Four RG-8 insulated cables were connected from the chamber electrodes to either side of the charging capacitor to reduce inductance. The vacuum characteristics of this chamber were good down to less than 500 microns of Hg, the limit of the pressure gauge used. Pressures as high as 20 psig were sustained in the chamber but movement of the lens holders were detected. This chamber yielded over 90% of the data gathered.

The metal chamber shown in Figure 6 was designed for the purpose of obtaining data at higher pressures. The top photograph of Figure 6 is a view looking through the 6 in. diameter access port. The polyethelene lens holders are shown above and below the spheres with one lens in place. The lens holders were designed for 2 in. or larger diameter lens with from $1\frac{1}{2}$ to $5\frac{1}{2}$ in. focal lengths. The lower photograph shows the exterior of the chamber. It was contructed in the form of a 12 in. cube, welded 3/8 in. steel plate. The case was completely insulated from both electrodes by nylon sleeves. One electrode is shown on the right side face. One side of the box contains the six inch access port while the remaining 3 faces have two inch diameter transparent windows of quartz or lucite $\frac{1}{2}$ inch thick identical to the top face shown. These three ports allow

analysis of the incoming and outgoing laser beams as well as simultaneous side viewing. The lucite windows had a transmittance of 93% at 6943 Å. The chamber was considered safe to 20 atmospheres but no data was taken above 45 psig.

Control-Diagnostic Equipment. The lasers and spark gap chambers were designed and assembled to insure generation of the necessary data to meet the experimental aims of the study. The actual observation and correlation of the parameters involved a much more complex system of control and monitoring equipment. This section will discuss the techniques used, grouping them as to laser control and monitoring, gap control and time delay measurement.

1. Laser: In Fig. 7 the pump light power supply provides the energy to fire the flashlamp and excite the ruby rod past its lasing threshold. The trigger wire initiates the flash and is controlled by a signal from the rotating prism so that the proper phase relationship is maintained between excitation and Q-spoiling. The determination of the optimum timing is described in Appendix A. In Fig. 8, the Kerr cell bias is removed a specified time after the pump light begins. The optimum delay setting must be determined experimentally in the same way as in the rotating prism case.

Diagnostic equipment for monitoring the laser pulse is also shown in Fig. 7 and 8. As the laser pulse immerges from the resonance cavity it strikes a 1/8 in. thick quartz plate oriented at 45 degrees to the beam. This beam splitter reflects

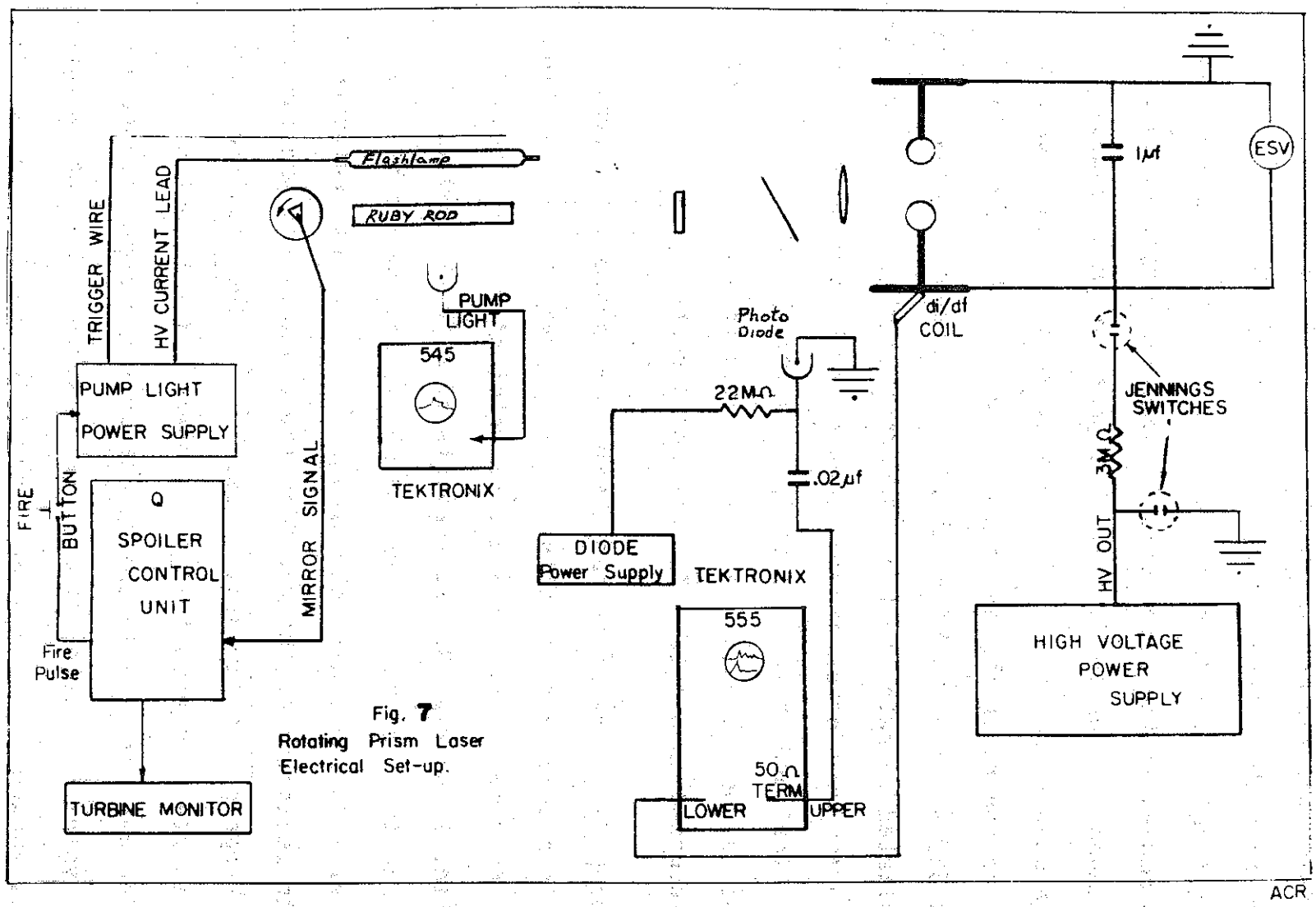

Fig. 7
Rotating Prism Laser
Electrical Set-up.

about 8% of the incident beam through several attenuating filters onto the cathode surface of a vacuum photodiode, hereafter called the laser diode. The instantaneous photocurrent produced at the cathode is directly proportional to the instantaneous laser intensity. The photocurrent produces a voltage change on the .02 MF capacitor which in turn sends a signal to the recording device. In the earlier work a Tektronix 555 scope was used as in Fig. 7. Faster response times necessitated changing to the 519 scopes in Fig. 8. In all cases the scopes operated on single sweep mode, triggered by the laser diode signal and photographically recorded by C-12 and C-19 Polaroid scope cameras. The actual scope traces of the data are discussed in Section VI, Data and Results.

2. Spark Gap: The spark gap chamber diagnostics involved determination of gap potential, chamber pressure, gap spacing and laser focus point. The gap charging circuit is shown in both Fig. 7 and Fig. 8. It consists of a 50 KV - 60 ma DC power supply to charge a 1 MF, 50 KV oil filled capacitor in parallel with the sphere electrodes. Two Jennings switches provide isolation of the gap from the power supply and furnish a discharge path to ground. A calibrated electrostatic voltmeter is placed across the gap to measure its potential.

The gas pressure in the gap chamber was regulated by a valve system consisting of a pressure gauge and a vacuum gauge. A small vacuum pump was used to purge the system. The gas to

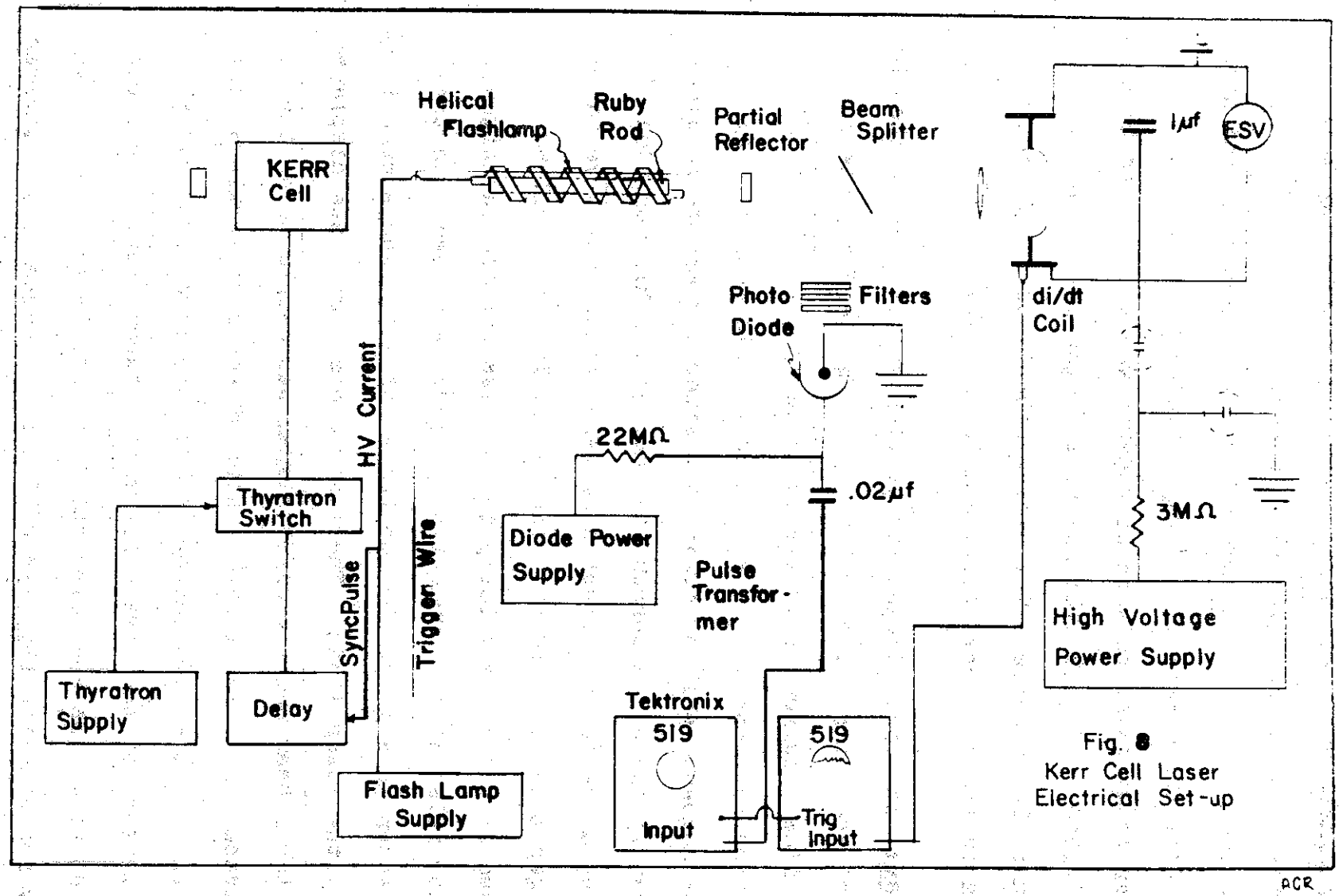

Fig. 8
Kerr Cell Laser
Electrical Set-up

be investigated was then inserted from a pressure tank until the desired chamber pressure was achieved.

The gap spacing was measured by a cathetometer placed about 20 feet from the spheres. Spacing could be read to within .1 mm. The laser focus point between the spheres was established by hitting a 1/1000 in. thick aluminum foil target in the gap with a preliminary laser pulse. The size of the focus spot and its position in the gap were determined in this way.

3. Delay: The final diagnostic problem was to measure the time delay between laser pulse arrival at the gap and the start of current flow. Current flow was detected by a small loop of wire placed near one of the electrodes. This loop goes by the name Rogowski coil or di/dt loop since any change in current near it induces a current in the loop. This was ideal for measuring a change in current from zero to some positive value as the gap began to conduct. The signal from the coil was displayed on a scope similarly to the laser photodiode signal. Two laser pulse-di/dt correlation methods were used. In the first, shown in Fig. 7, the two traces of a 555 scope were triggered by the laser diode. The laser diode signal was displayed on the lower beam and the di/dt signal was displayed on the upper trace. Both input cables were of the same length so comparing the two beam displacements from the zero line gave a direct measure of the time difference between them. The sweep speed and rise time characteristics of the 555 were not satisfactory for use with the Kerr cell laser because of its shorter

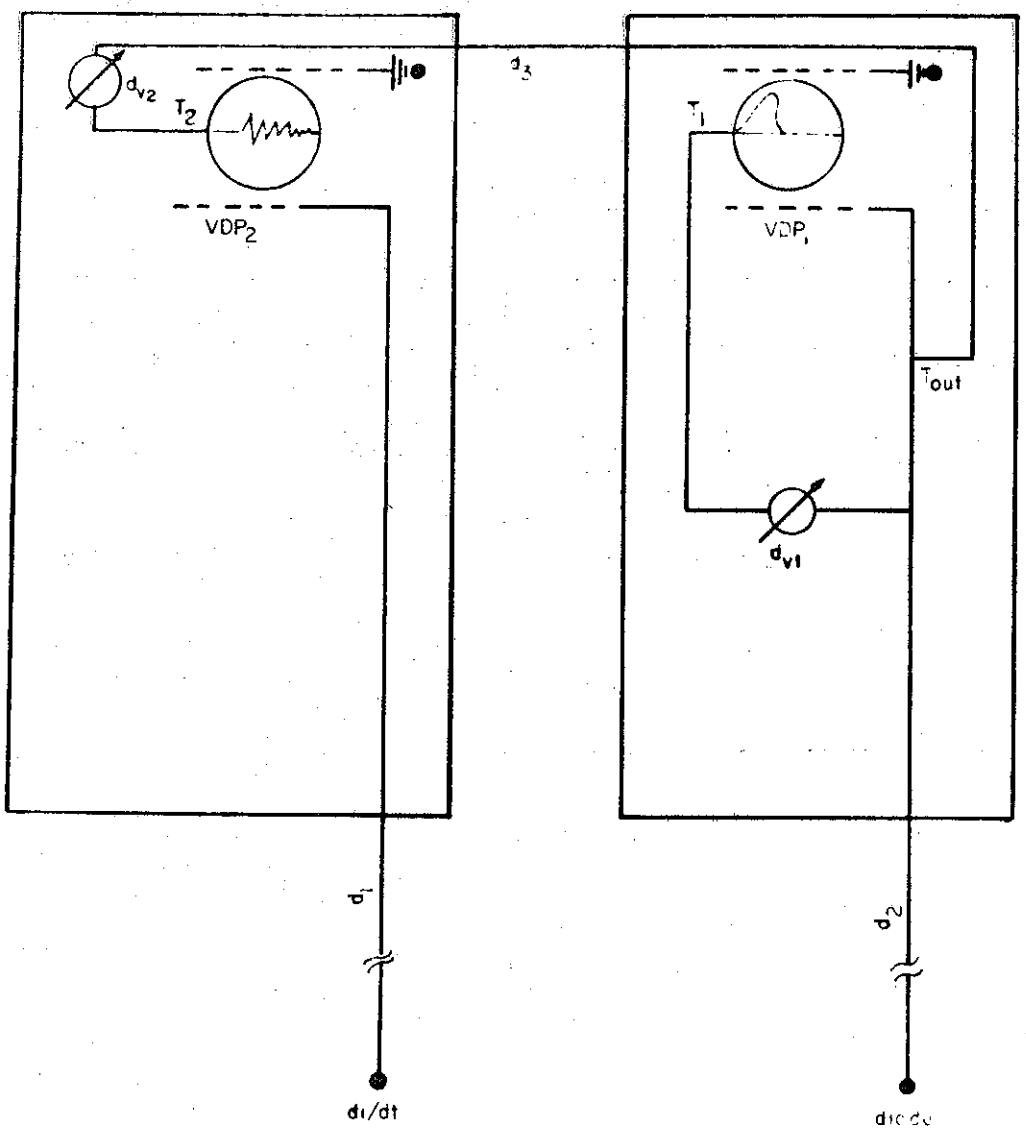

d_1= delay between di/dt origin and vertical deflection plates of scope 2 (VDP_2)

d_2= delay between diode and scope 1 output trigger

d_3= delay between output trigger of scope 1 (T_{out}) and d_{v2} pot of scope 2

d_{v2}= variable delay between input trigger signal and actual scope trigger

*** Set d_{v2} so that: $d_1 = d_2 + d_3 + d_{v2}$

Fig. 9 Dual Scope Synchronization for di/dt Delay Measurement

output laser pulse. The dual scope method shown in Fig. 8 was then devised with excellent success. The left scope was triggered by the laser diode as before. An output trigger signal from this 519 was used to trigger theright 519 scope displaying the di/dt signal. Thus, by knowing the various internal delays of the cables and scopes a correlation between the two signals was possible.

It was considered too difficult to determine the actual delays in each component of the signal paths so a method was used to measure the time relationship of two known signals coming to the scope, namely, a single pulse sent through both cables and being displayed on both scopes. Figure 9 gives a schematic picture of the set-up. The procedure is simple. Simultaneously inject a signal into the di/dt cable at the gap and the laser cable at the diode. Adjust the internal delays of the scope so that both pulses are displayed at t=0 on the trace. This is the case when $d_1 = d_2 + d_3 + d_{v2}$ as indicated on Fig. 9. Therefore, if the di/dt signal is in fact delayed somewhat from when the laser occurs, this additional delay will cause the signal to reach the vertical deflection plates of second scope after the trace has begun to sweep. A measure of the delay is read directly and converted to time according to the set sweep speed. Sample traces are included in the next section. A correction of this number must be made to account for the time it took the laser to go from the beam splitter to the spark chamber.

Fig. 10 Assembly Instructions CT-SIP

To give the reader an idea of how this apparatus was assembled in the lab, a photograph of the experimental set-up is shown in Figure 10 to correspond to the schematic representation of Figure 7. The various parts are labeled as follows:

1. Laser flashlamp and ruby rod holder
2. Rotating prism turbine
3. Q-spoiling control unit
4. Flashlamp photodiode monitor
5. Beam splitter and laser diode assembly
6. Electrostatic voltmeter
7. Spark gap high voltage power supply
8. Gap charging capacitor
9. Jennings isolation switch
10. SF_6 fill gas supply
11. Chamber evacuation pump
12. Spark gap chamber

The oscilloscopes used to record the signals were located in the adjoining room to cut down on the stray fields produced during gap triggering.

IV. Data and Results

In the previous sections the parameters were explained and the methods used to obtain the measurements were discussed. This chapter will deal with the actual data gathered from the experimental assembly. Samples of raw data are given, most of the reduced results are displayed in graphical form.

Oscillograms

The primary source of raw data was from oscillograms of scope traces. Several sample traces are shown in Fig. 11 and 12. Figure 11 is an example of the single dual beam 555 scope data for relating laser pulse-di/dt signals. The necessary scope settings required for proper interpretation are listed beside the oscillogram. It is an easy matter to convert linear distance between start of the laser pulse signal and the di/dt signal to obtain Δt_D. For this example the time delay is calculated to be 340 ns. An example of the dual scope data is given in Fig. 12. Here, the upper oscillogram shows the output of the laser diode and the bottom one displays the di/dt signal. Having followed the synchronization prodedure explained in the last chapter, the time delay Δt_D is calculated from the sweep speed and the linear distance from triggering to di/dt appearance. The delay for this case is seen to be about 100 ns. No grid is shown on the lower trace so as not to interfere with the data. The oscillograms were calibrated: 1 scope centimeter = 1.03 oscillogram centimeter.

The traces containing the laser diode output supply the

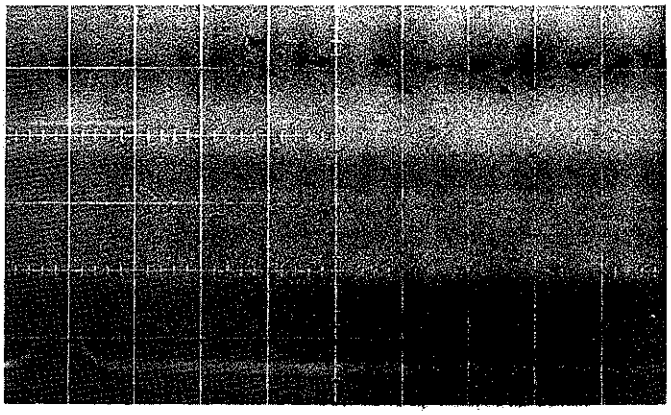

Upper Trace
(di/dt)

Trigger: lower beam
Amplitude: 5 v/cm
Sweep speed: 200 ns/cm

Lower Trace
(laser)

Trigger: self
Amplitude: 5 v/cm
Sweep speed: 200 ns/cm

Fig. 11 Single 555 Scope Delay Oscillogram

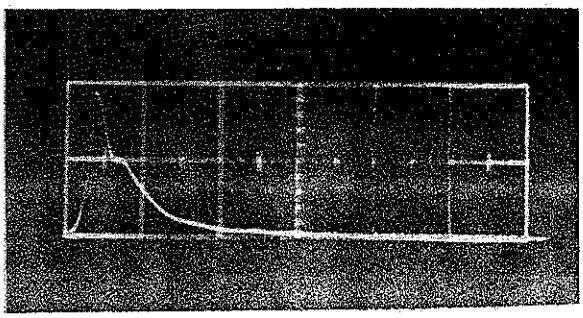

Scope #1
(laser)

Trigger: self
Amplitude: 9.5 v/cm
Sweep speed: 20 ns/cm

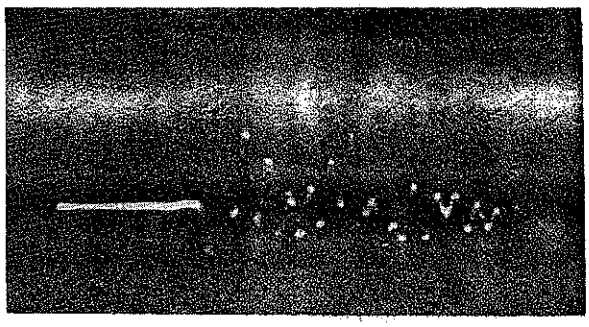

Scope #2
(di/dt)

Trigger: scope #1
Amplitude: 8.9 v/cm
Sweep speed: 50 ns/cm

Fig. 12 Dual 519 Scope Delay Oscillograms

necessary information to determine the energy and power in the pulse. The techniques used for calibrating the oscillograms for these parameters are explained in Appendix A.

For the sake of convenience and sound procedure, the backs of the oscillograms were used to record all pertinent data for the particular shot: gap potential and spacing, gas pressure, self breakdown voltage, and beam focus point. These numbers were then transferred to a columnar data sheet for easier handling. After the time delays were calculated the data was then plotted in graphical form for interpretation.

Graphs

Figures 13 through 22 show the characteristic ways the data was graphed. These specific ones are included here as representative of the general behavior observed throughout the study. Appendix B contains similar graphs of the remaining data and serve to substantiate the conclusions presented in the Discussion section.

Figures 13 and 14 show the dependence of time delay Δt_D on the laser beam power for given spark gap conditions, i.e. constant E_g/p. The two graphs display data obtained with the rotating prism and Kerr cell lasers respectively. Thus both low and high power regions were covered.

Figure 15 shows a plot of time delay versus the generalized gap parameter E_g/p. This ratio of gap electric field to gas pressure is a common one used in delay studies because it expresses the trade-off between electron accelerating force

and mean free path between collisions. The comparison between behavior in air and N_2 is intended here. Figure 16 gives the data obtained for SF_6 under similar conditions. The dielectric strength of SF_6 is about two times that of N_2 so the E_g/p value near self breakdown is considerably higher.

Figure 17 shows the delay behavior as a function of E_g/p for different values of pressure. The vertical lines labeled SB are the values of E_g/p for self breakdown at that pressure. Figure 18 is a semilogarithmic plot of the same data.

It was of interest to determine if incident ultraviolet light on the gap would affect the delay characteristics. A mercury arc lamp in a quartz envelope was shined through a quartz window in the vacuum chamber lens holder. The data in Fig. 19 shows behavior with and without ultraviolet.

The output light pulse from the laser was linearly polarized. To determine if the polarity orientation of the laser beam with respect to the gap electric field was an important feature of the triggering, the data in Fig. 20 was obtained. The entire Korad laser resonance cavity was rotated 90 degrees to achieve the perpendicular orientation.

As mentioned earlier, one of the possible variables was the focus point location within the sphere-sphere gap. A plot of t_D versus E_g/p with d_n as parameter is given in Fig. 21. The quantity d_n is the distance between the focus point and the surface of the cathode (-) sphere.

Figure 22 represents a convenient way of presenting switch

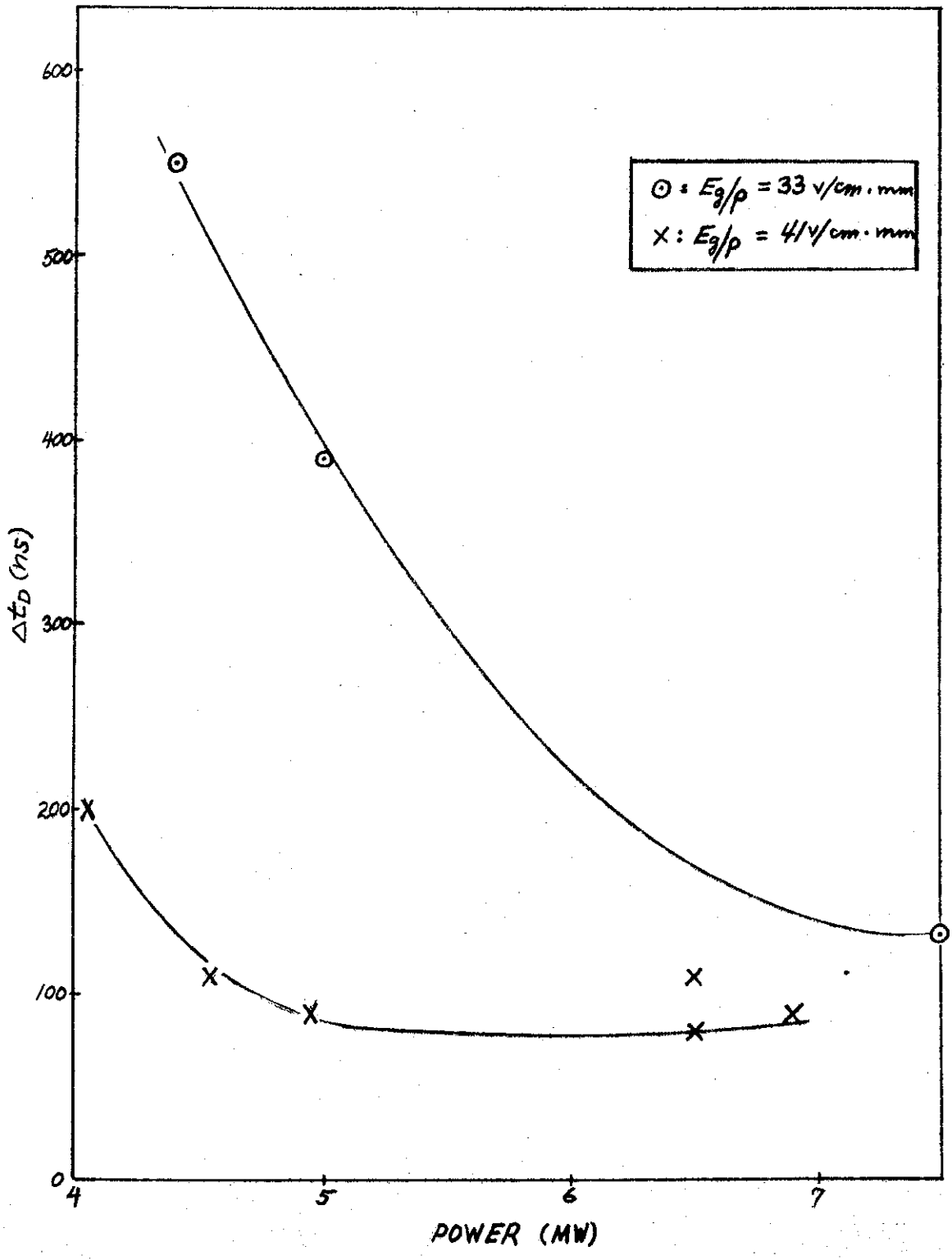

Fig. 13 Δt_D vs Power

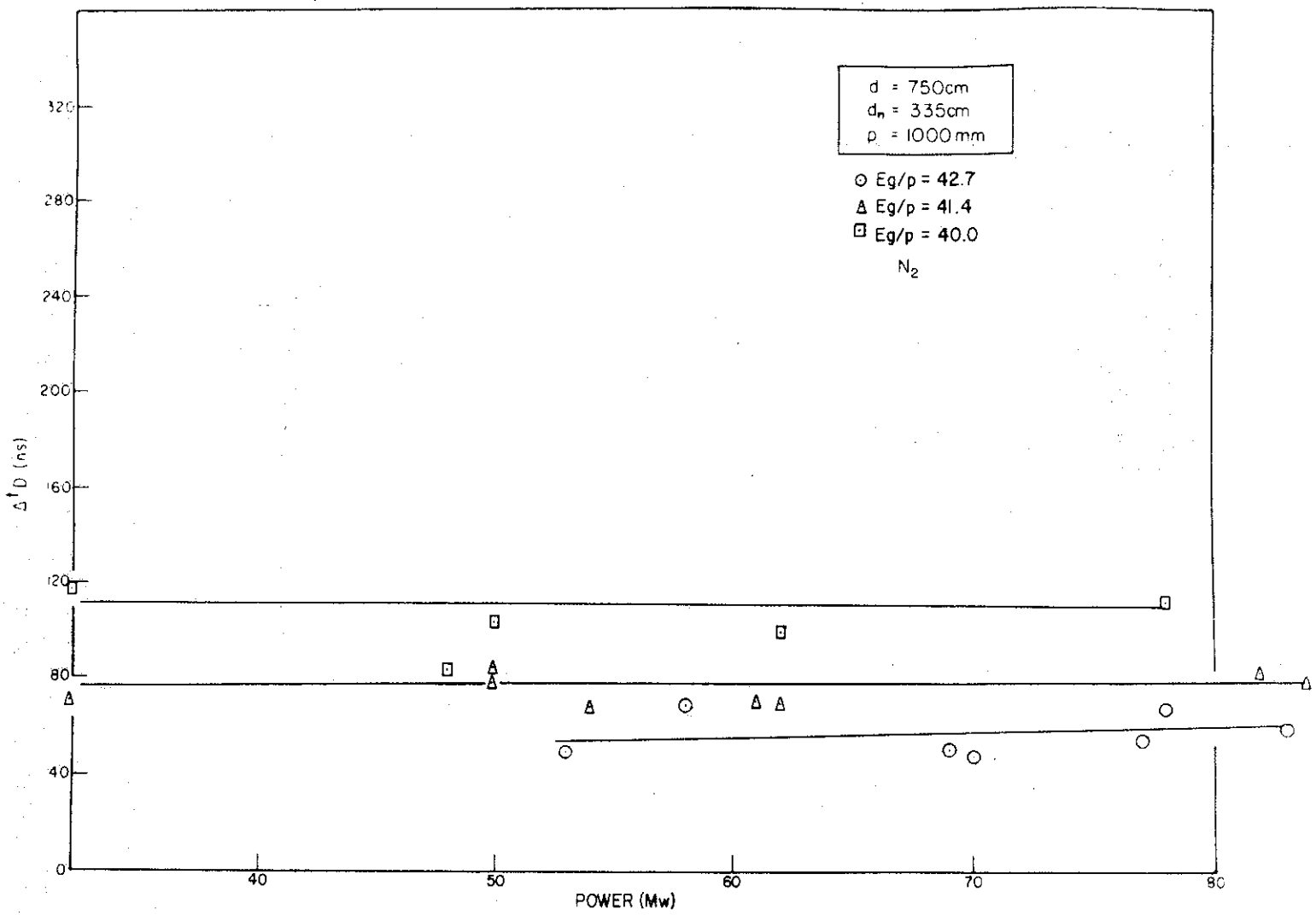

Fig. 14 Δt_D vs Power d, d_n, p constant

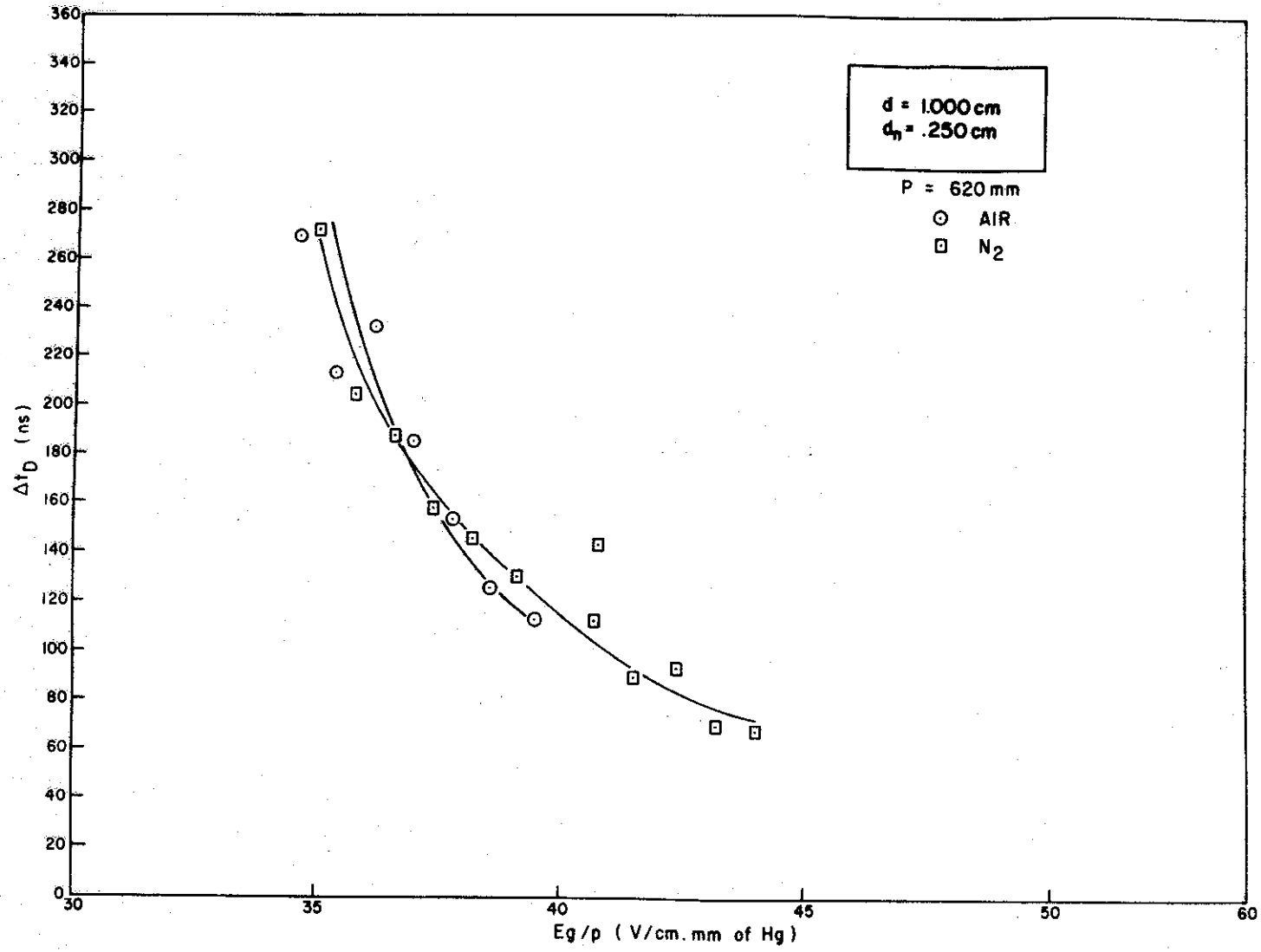

Fig. 18 Δt_D vs E_g/p d, d_n, p constant

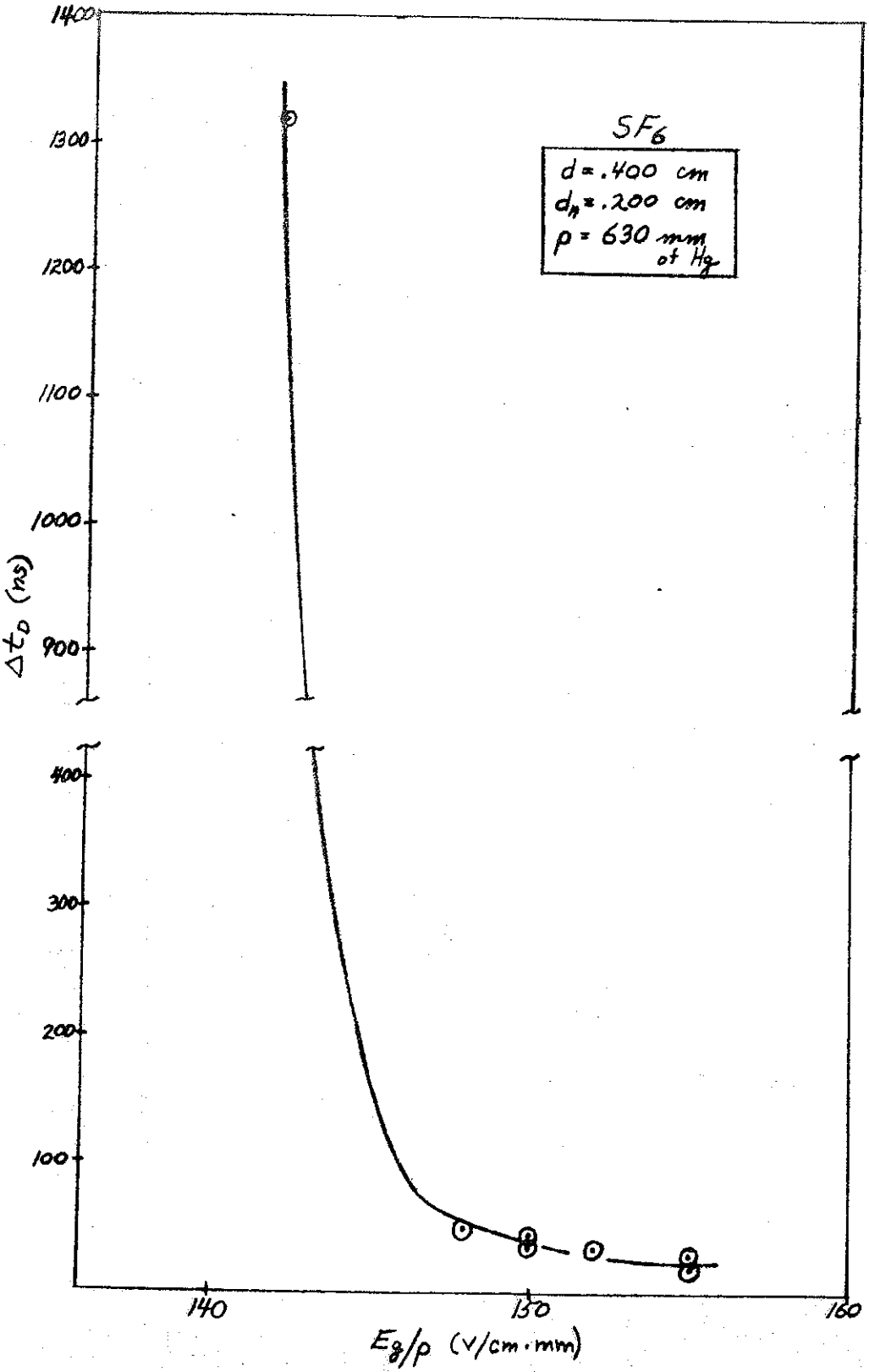

Fig. 16 Δt_D vs E_g/p d, d_n, p constant

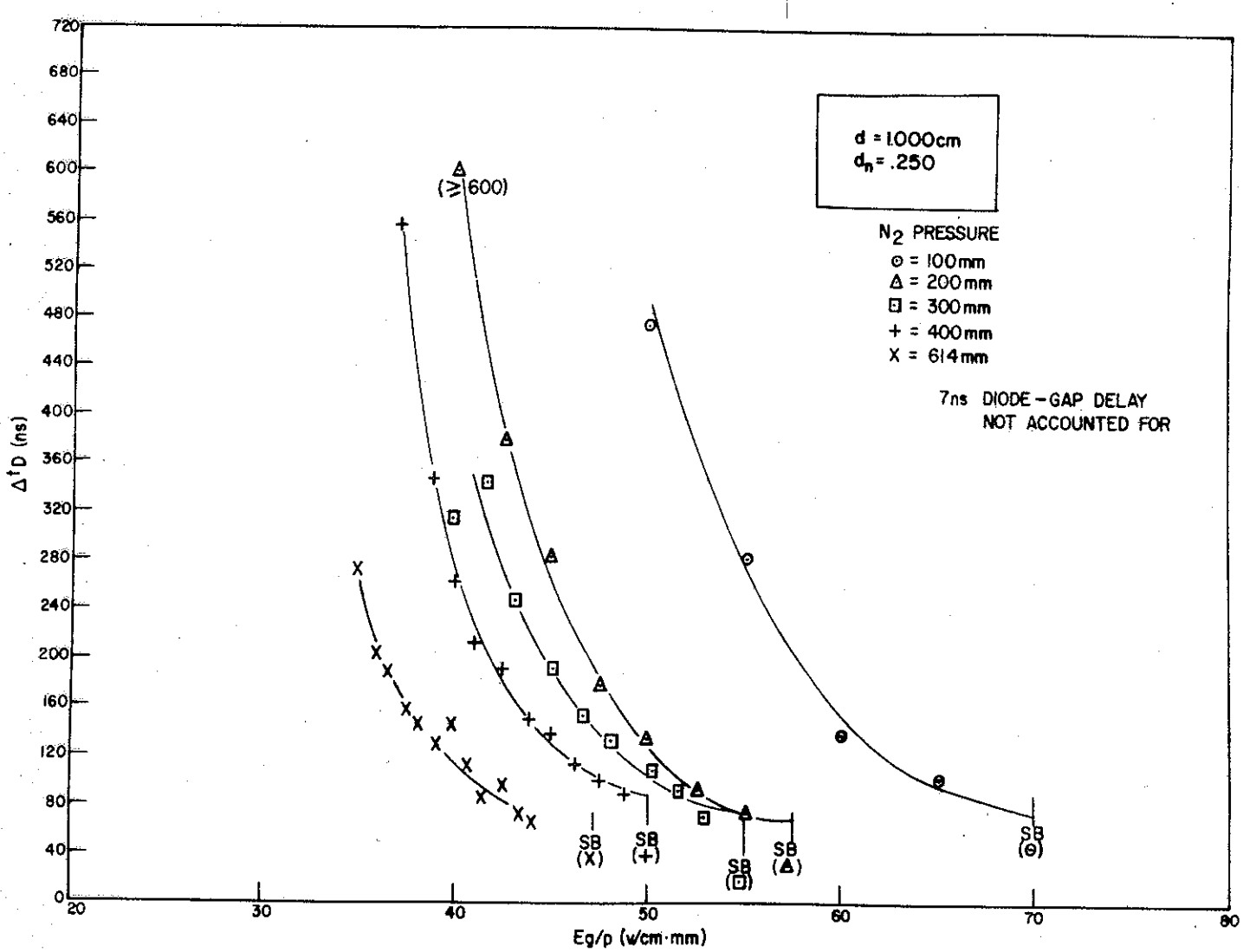

Fig. 17 Δt_D vs E_g/p (N_2) d, d_n constant

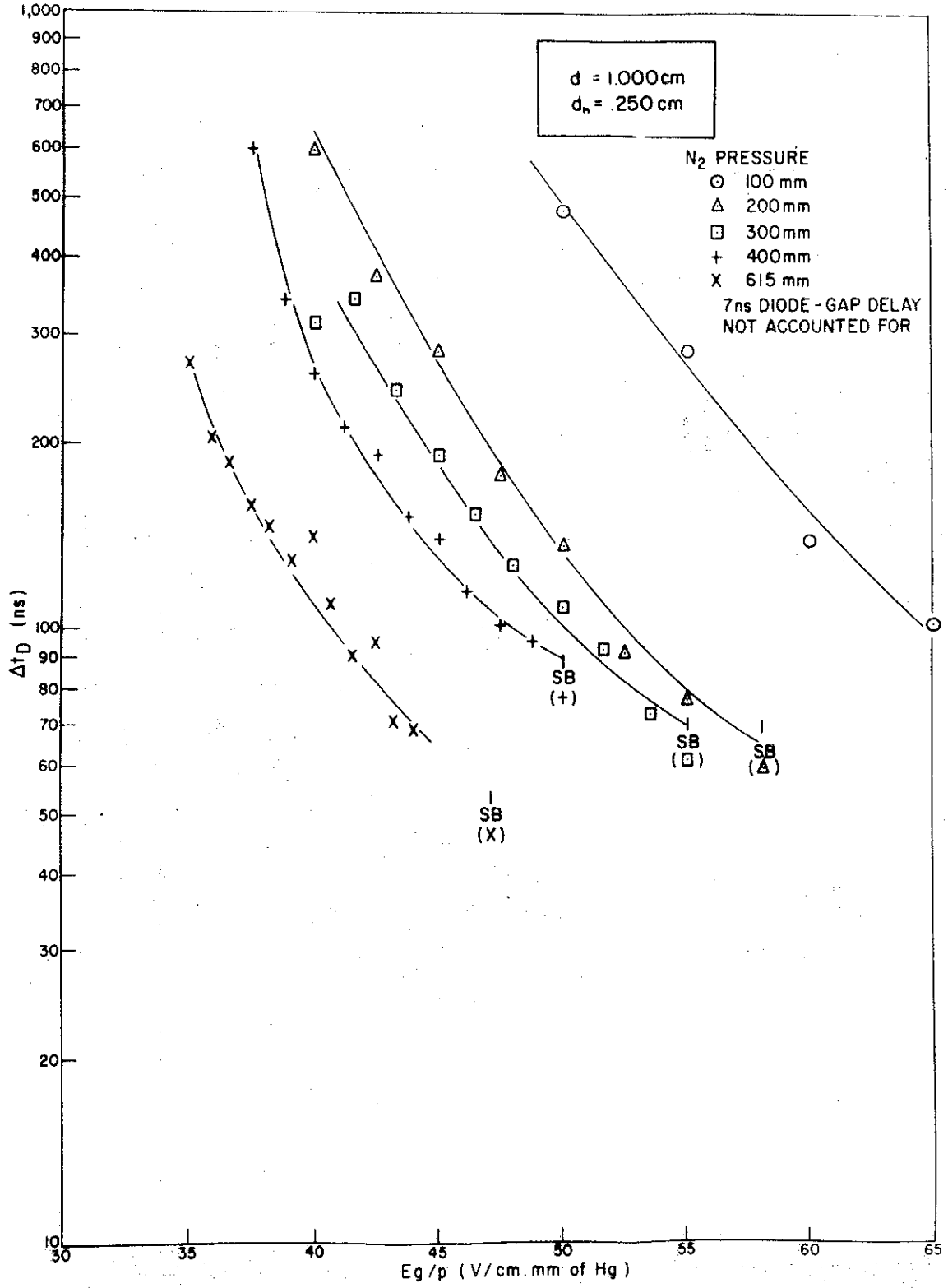

Fig. 18 $Ln\Delta t_D$ vs E_g/p (N_2) d, d_n constant

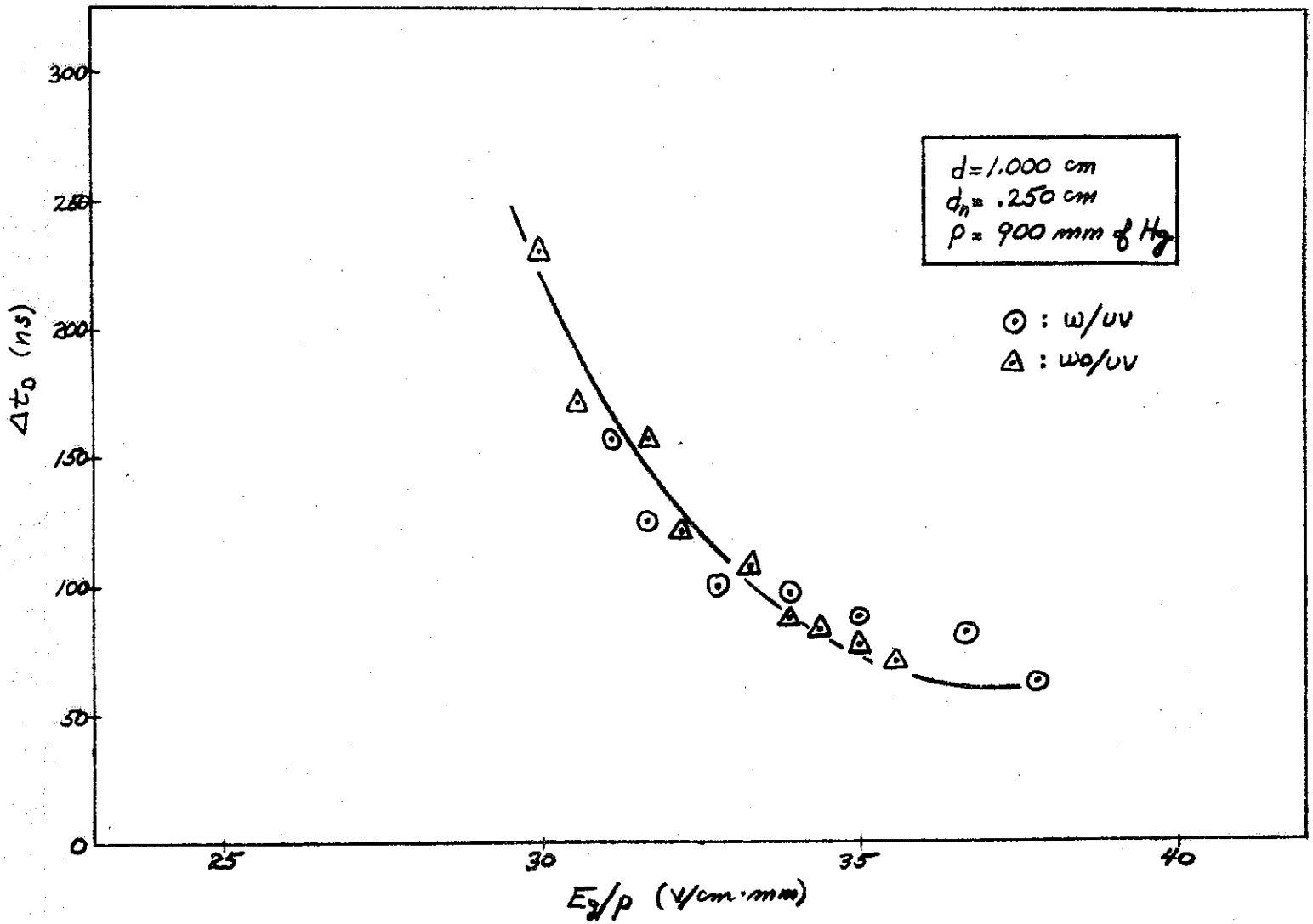

Fig. 19 Δt_D vs E_g/p d, d_n, p constant

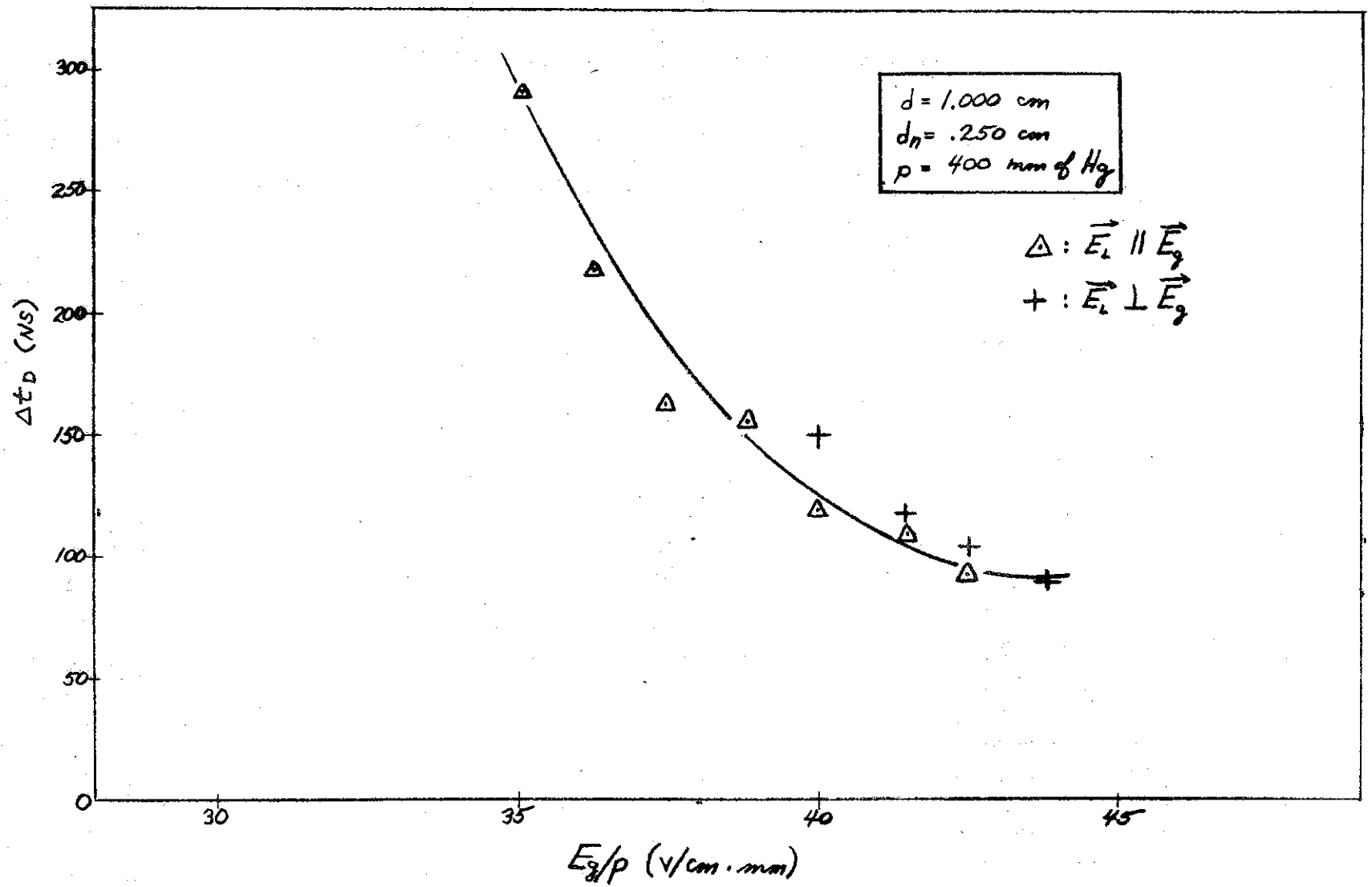

Fig. 20 Δt_D vs E_g/p d, d_n, p constant

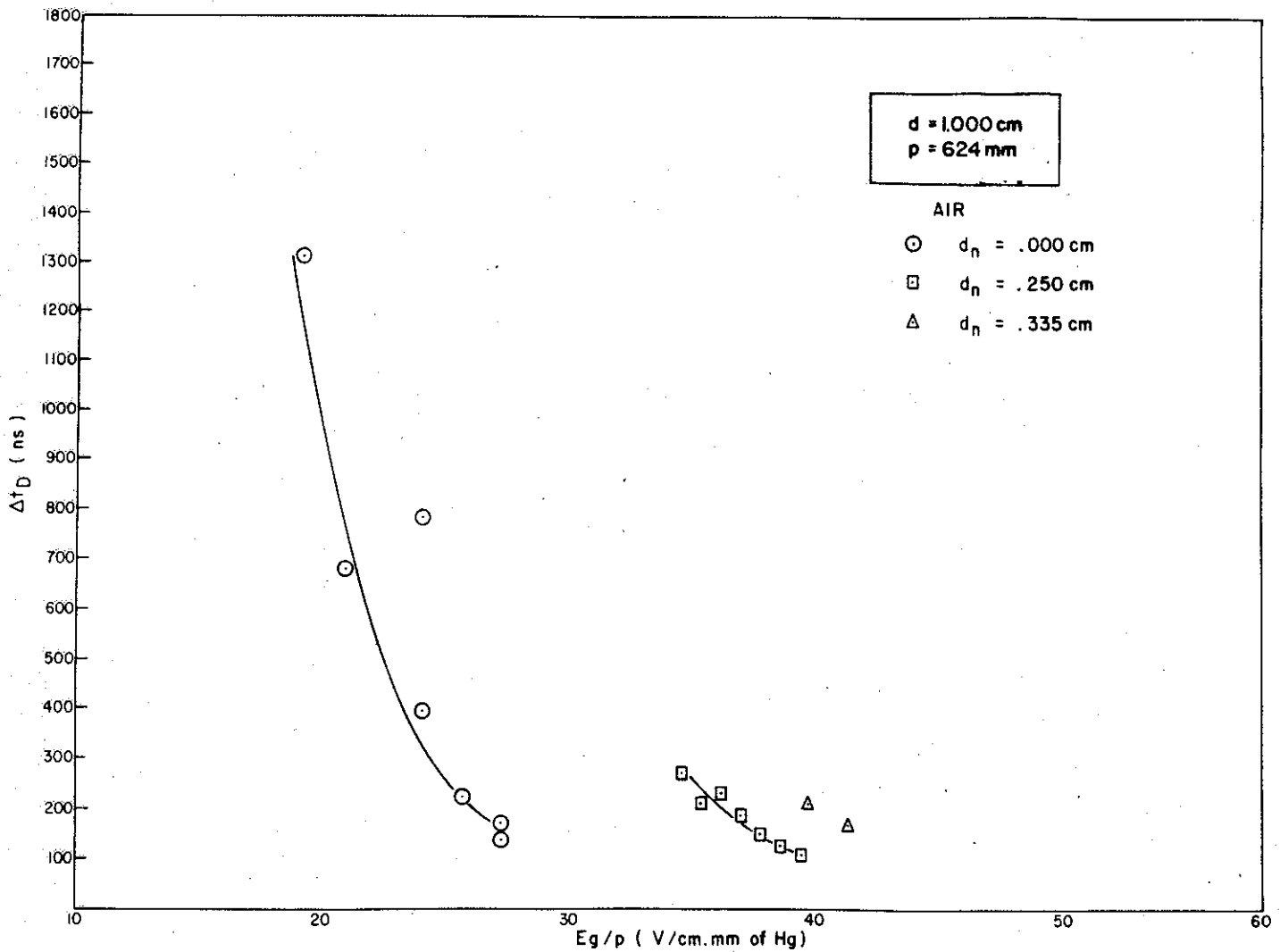

Fig. 21 Δt_D vs E_g/p (AIR) d, p constant

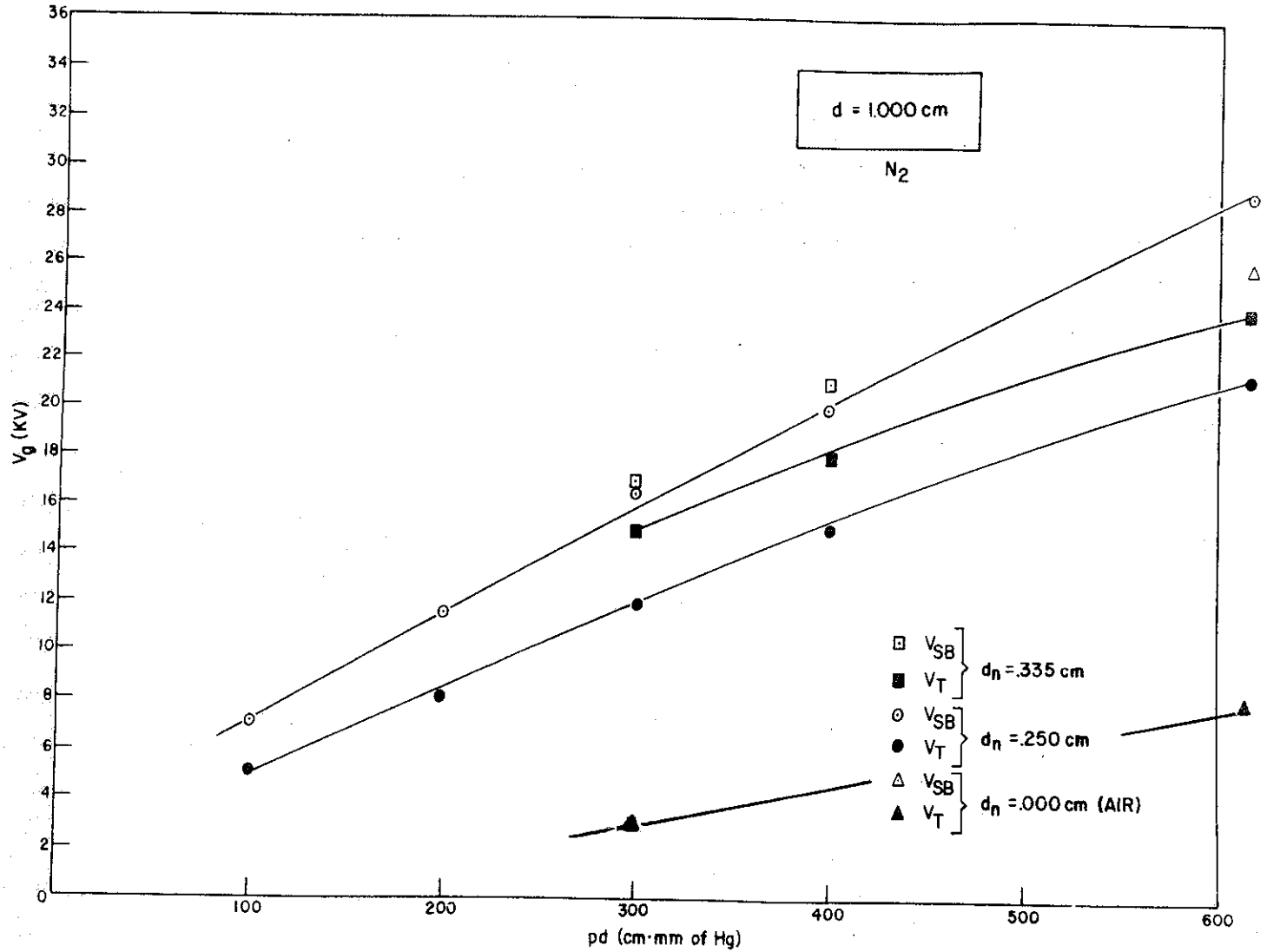

Fig. 22 V_{SB} & V_T vs pd (N_2) d constant

data. It is a plot of the electric potential between electrodes versus the product of gap spacing and gas pressure (pd). The upper curve is Pachen's curve relating the self breakdown voltage of the gap as a function of pd. The lines beneath it show the lower limit of voltage at which the gap was triggerable with the laser beam for different values of d_n.

Error Analysis

An important part of any experimental investigation is the estimation of the errors in the measurements. This section will discuss the errors introduced by the laser, oscilloscopes and spark gap diagnostics. Comments will also be made about the jitter of the switch or the mean fluctuation about the average delay time.

Laser. Twenty Kerr cell laser shots were taken at evenly spaced time intervals and the energy of each was measured. All prefire conditions were the same, yet different outputs were observed. The average output energy for the series was .7 joules as determined by the calibration curve, Fig. A-4, Appendix A. The variance was calculated to be $\pm$.1 joules or a relative uncertainty of about 14%. Most of the data obtained with the Kerr cell, high power laser was correlated at constant beam energy. The effect of this 14% variation is probably small considering the non-power dependence displayed in Fig. 14. The uncertainty in the actual laser beam energy for a single shot is about 15% due to the calibration technique used.

Oscilloscopes. Oscilloscope errors arise from fluctuation in triggering behavior and the limit of error in measuring the oscillograms. The dual 519 scope triggering variation was tested by simulating a shot with the Model 961 pulse generator. Five shots were displayed on the same oscillogram at 10 ns/cm and no difference was measurable between each shot. The reproducibility of the scopes was thus established. The uncertainty in Δt_D which can be associated with the scope is the error in measuring the time to current flow. With an eyepiece millimeter scale trace lengths were determined to within $\pm$.2 mm. Thus for a 10 ns measurement on the 10 ns/cm sweep speed the error would be $\pm$.2 ns or $\pm$2%.

Spark Gap. The error in measuring the gap spacing, d, can be estimated as about $\pm$.1 mm for a spacing of 1 cm. The instrument limit of error of the cathetometer is less but optical distortion and poor sphere illumination would increase the error. Beam focus point could be determined within $\pm$.1 mm by using the magnifying scale eyepiece. Gas pressure in the gap was read with a vacuum gauge good to within about 3% and a crude pressure gauge no better than 10%. Perhaps the most uncertain measurement of all was the gap potential. The calibrated electrostatic voltmeter has an instrument limit of error of only 2% but the fluctuation in voltage from the DC power supply could not be established. This random variation may account for a considerable portion of the delay jitter present. For typical values of the measurements the uncertainties were:

E_L = .7 ± .1 joules (±14%)

t_D = 50 ±2 ns (±4%)

d = 1 ±.01 cm (±1%)

d_n = .5 ±.01 cm (±2%)

V_g = 30 ±.6 KV (±2%)

p = 1000 ±100 mm of Hg (±10%)

E_g/p = 40 ±5 v/cm mm of Hg (±12%)

Switch Jitter. All of the above uncertainties will ultimately be felt in a variation in the time delay Δt_D. Since the nature of the phenomenon is not fully understood, it is difficult to relate the observed jitter to the measured parameters. The magnitude can be determined however. For each of the twenty laser shots used to establish the output uncertainty a delay measurement was made. For ten of the shots the pressure was such that the average delay was 39.7 ns. The variance was calculated to be ±4.2 ns or a relative variation of ±11%. For ten shots taken at a lower pressure the average delay was 73.7 ns with a variance of ±5.4 ns (±7.3%). Under more controlled conditions it is believed possible to reduce the jitter considerably. There may be a statistical fluxuation as in the case of overvoltage triggered switches which would set a lower limit.

V. Discussion and Conclusions

On the basis of this investigation it has been shown that certain of the switch characteristics desired by AFWL (see Section I) can be achieved by the laser beam triggering of a spark gap. With respect to the short delay times desired, the experimental results show that response times vary inversely with gap electric field, gas pressure and focus distance from the anode. Delay times of 20 ns were observed; shorter delay times were present but could not be measured. No dependence on laser power or polarization was observed. The results as displayed in Figs. 13-22 will now be discussed in more detail.

Figures 13 and 14 indicate that the triggering response times show a marked laser beam power or energy dependence from zero to about ten megawatts then becomes insensative to changes in laser beam variation. There definitely is a triggering threshold which varies with gap parameters but no careful study was carried out. It should be noted that short delay times favor higher values of E_g/p.

Figure 15 shows the negligible difference observed in behavior for air and N_2 in the gap. It also shows the general behavior of delay versus E_g/p. Again shorter delays are obtained for higher E_g/p values. Figure 16 shows that even shorter delays (20 ns) were obtained in SF_6 at the same pressure. Higher electric fields in the gap are possible with SF_6.

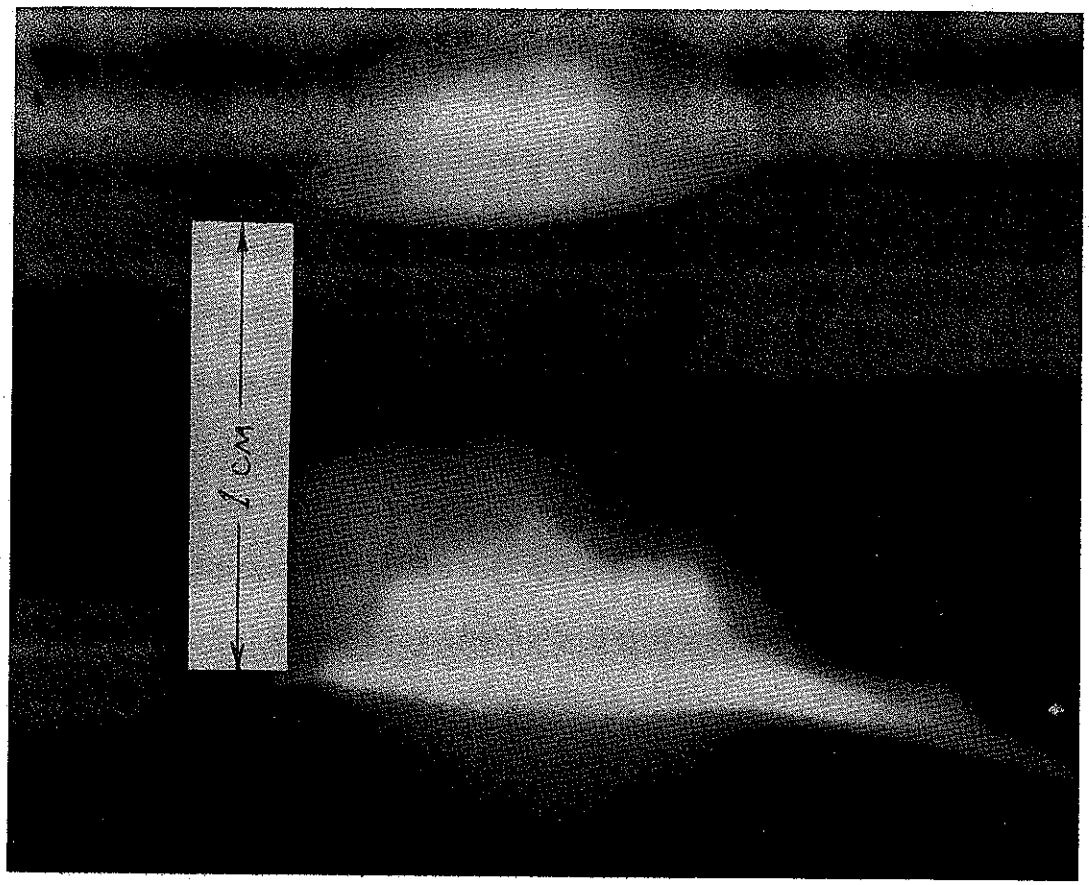

Fig. 23 Laser Induced Photoemission

Figure 17 is a parametric display with respect to pressure. For a given E_g/p value shorter delays are obtained at the higher pressures. It must be mentioned that the electric fields are higher also. For all pressures it appears that the lower delay limit occurring at the self breakdown line is about 80 ns. This may not necessarily be true at much higher pressures. The same data in Fig. 18 shows a slight curvature on a semi-logarithmic plot.

Figure 19 indicates the negligible influence of ultraviolet light shining on the gap. In considering this result and the focused UV technique usually used, it is apparent that intensities were not high enough to make a suitable determination of the UV effect.

The effect of laser polarization is likewise indicated to be negligible according to Fig. 20. This may mean that the electric field intensity at the focus point does not affect the gap voltage and does not influence the gas ionization. It is conceivable that in a polarized liquid or solid dielectric the laser beam polarity could have a sizeable influence.

Figure 21 has some interesting information. It indicates that the closer the triggering initiation is to the cathode the faster the response times. This could be due to the shorter cathode travel distance of the positive streamer. In the case where the laser beam was focused directly on the cathode, d_n = .000 cm, a visible photoemission was observed which extended about .3 cm from the cathode (see Fig. 23). In Fig. 21 the d_n = .000 cm line ends at about E_g/p = 27 v/cm·mm because of

experimental difficulty encountered with noise interference at these low delay times. The lower delay limit is believed to be quite small at higher voltages. (Placing the spark gap chamber in an electrically isolated screen room would probably eliminate the noise problem.)

Unlike existing switches which require overvoltages to trigger, this technique enables one to trigger a gap which is never charged to the self breakdown voltage. Figure 22 illustrates this fact. It is noted that the width of the triggering region is a function of the laser beam focus point in the gap.

In order to correlate the data obtained with the two existing theories of arc formation a simple calculation is made using the propagation velocities given in Section II and the measured delays in SF_6. Let us say the Townsend avalanche was initiated at the midpoint of a .4000 cm gap charged close to self breakdown, i.e. the situation in Fig. 16. Let us also assume the avalanche moves at its terminal velocity of 2×10^7 cm/sec, toward the anode and that after moving .1 cm the positive space charge field at the center of the gap can form the streamer toward the cathode. Assuming its terminal velocity as 10^9 cm/sec, the total delay time for gap closure would be:

$$\Delta t_D = \frac{.1 \text{ cm}}{2 \times 10^7 \text{ cm/sec}} + \frac{.2 \text{ cm}}{1.3 \times 10^8 \text{ cm/sec}} + \frac{.4 \text{ cm}}{10^9 \text{ cm/sec}} = 7 \text{ ns}.$$

From Fig. 16 a delay of about 20 ns was obtained. Considering the rather abrupt behavior of the example and the vast uncertainties in the velocities used, the agreement is reasonable.

If one assumes a completely Townsend process employing the much slower positive ions without streamer formation, a minimum time delay is calculated to be:

$$\Delta t_D = \frac{.2 \text{ cm}}{2 \times 10^7 \text{ cm/sec}} + \frac{.2 \text{ cm}}{2 \times 10^4 \text{ cm/sec}} = 10^{-5} \text{ sec } (10 \mu\text{s}).$$

This is the same orderof magnitude as the formative time lags observed in low pd discharges where the Townsend theory is applicable.

Clearly, if one is searching for a reasonable model for the laser triggering of a spark gap at high pressure the best available model is the streamer theory. In the opinion of the author the laser initiation of the arc discharge is not only a useful phenomenon for switching but will be ideal for basic studies of arc formation once enough information about laser beam-gas, metal interactions is known to accurately describe the free electron formation. Suggestions for continued study of the switch problem are given in the following section.

VI. Recommendations

The series of experiments covered by this report has supplied enough information to guide future studies and has shown the need for additional diagnostic techniques.

One of the major areas needing attention is the detailed time behavior of the arc formation once the laser beam has initiated the process. A number of available tools could be used. The volt-ampere characteristics of the discharge as a function of time could be determined by existing techniques (Ref. 1:1117-1118). Correlated with this could be more direct observation of the discharge by time resolved spectroscopy and high speed photography. This would yield extremely valuable information concerning the ionization process and arc propagation and expansion velocities.

More detailed study of the laser beam would be fruitful, especially an analysis of the beam immerging from the spark gap chamber after the triggering process has been initiated. A satisfactory procedure is described in Ref. 8:5. Use of higher power lasers would also be of significant importance. If the optical breakdown threshold of the gas is surpassed a pronounced effect on the switch behavior may be observed.

One of the conclusions inferred from this study is that the primary parameter effecting the response time is the electric field strength in the gap. Since this is limited by the dielectric material between the electrodes the natural extension of using SF_6 at high pressure is to use liquid or even solid

dielectric materials in the gap. Numerous oils and crystals with good optical properties are available.

For improving switch response as such, several different gap-laser configurations could be tried. A multiple beam splitting-focusing arrangement could be devised that would simultaneously initiate the triggering process at different points between the electrodes. Presumably this would greatly reduce the formative time lag of the arc formation. A similar condition might be achieved by injecting a higher power laser beam axially through the chamber electrode.

It is felt, however, that more research on a basic level is needed. It was suggested that perhaps using pure monatomic gases of low Z number such as Helium, Neon and Argon would greatly simplify the theoretical considerations and lead to better understanding of arc formation mechanisms in general.

Bibliography

1. Bandel, H.W. "Measurement of the Current during the Formative Time Lag of Sparks in Uniform Fields in Air." Physical Review, 95:1117-1125 (September, 1954)

2. Damon, E.K., and R.G. Tomlinson. Ionization of Gases by Optical Maser Radiation. Antenna Laboratory Report No. 1085-19. Columbus, Ohio: Ohio State University, November 30, 1962.

3. Fisher, L.H., and B. Benderson. "Formative Time Lags of Spark Breakdown in Air in Uniform Fields at Low Overvoltages." Physical Review, 81:109-114 (January, 1951).

4. Lichtman, D., and J.F. Ready. "Laser Beam Induced Electron Emission." Physical Review Letters, 10:342-345 (April, 1963).

5. Lengyel, B.A. Lasers. New York: Wiley, 1962.

6. Loeb, L.B., and J.M. Meck. The Mechanism of the Electric Spark. London: Oxford University Press, 1941.

7. Meek, J.M., and J.D. Craggs. Electrical Breakdown of Gases. Oxford: Clarendon Press, 1953.

8. Meyerand, R.G., and A.F. Haught. Research on the Electrical Breakdown of Gases Under Intense Optical Illumination. United Aircraft Corporation Research Laboratory Report No. C-920088-2. East Hartford, Conn., January, 1964.

9. Smith, L., "Two-Photon Photoelectric Effect." Physical Review, 128: 2225-2229 (December, 1962).

10. Tomlinson, R.G., and E.K. Damon. Analytical Comparison of Several Techniques for Determining Parameters of Laser-Induced Ionization. Antenna Laboratory Report No. 1083-21. Columbus, Ohio: Ohio State University, November 30, 1962.

Appendix A

System Alignment and Calibration

Alignment

Optical alignment of laser components is extremely critical and greatly effects the quantity and quality of the coherent light pulse produced. Figure A-1 shows the alignment assembly. A mercury arc lamp mounted in a metal box shines through a .05 in. diameter hole located at the focal point of a lens. This point source-lens system produces a collimated light beam in the horizontal plane of the ruby rod. This alignment beam strikes the beam splitter and is reflected down the optical axis of the laser. This, then, establishes the reference axis. The ruby rod is placed on axis and adjusted until the front flat reflects the alignment beam back on itself. The return beam passes through the beam splitter and is focused onto a white plate. This is called the reference spot. The rotating prism turbine is then adjusted until the return beam off the total internal reflective surfaces is focused at the reference spot. Next, the front reflector is installed and adjusted until its reflected signal falls on the reference spot. At this point the return signal from the prism, rod, and front reflector are all focused at the same point. This means that the three surfaces are on axis and parallel, the condition for proper alignment. To place the spark gap chamber in alignment the lens and focus plate are removed and the chamber is adjusted until the laser reflected signals are centered on the chamber focusing lens. The entire system is now in proper alignment.

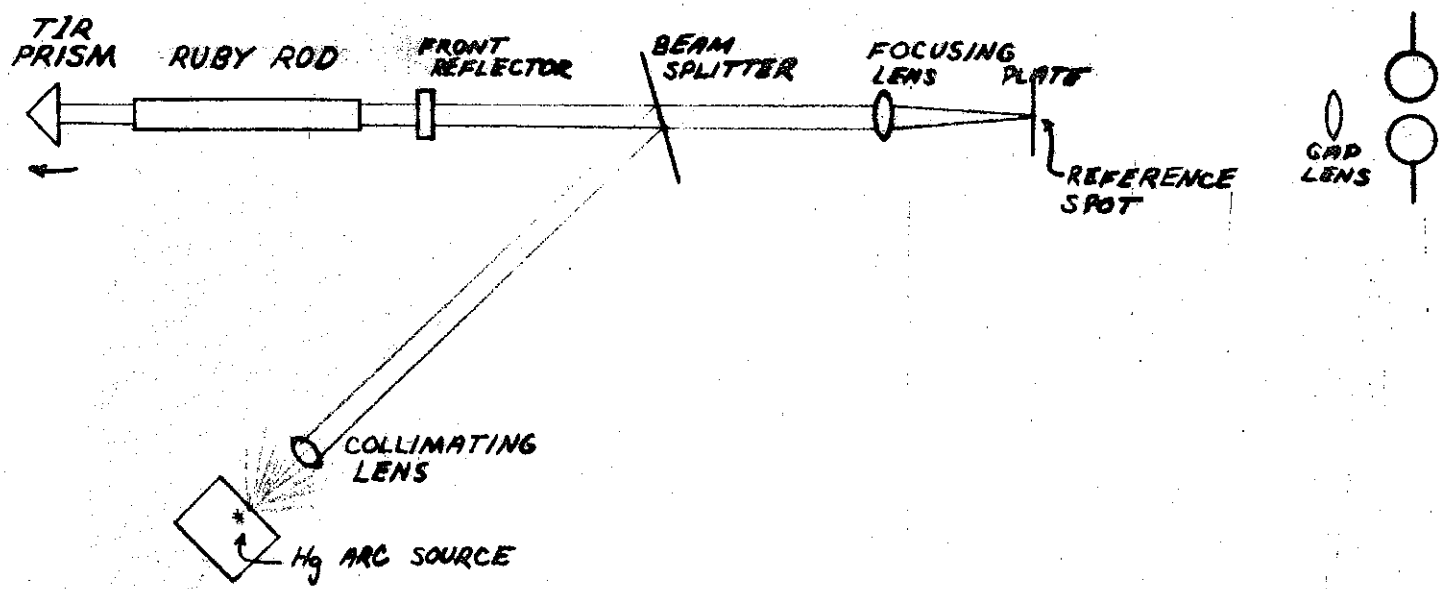

FIG. A-1
ALIGNMENT SYSTEM

Q-Spoiling Optimization

For the rotating prism laser it was necessary to determine the proper time delay between start of the flash lamp and Q-switching to obtain the maximum output. This was done by systematic variation of the delay until the maximum output was established. The time relationship was established by using a pump light monitoring photodiode, the output of which was displayed on a Tektronix 545 scope. The diode was placed in such a position that it would also detect the laser output. A typical oscillogram is shown in Fig. A-2. It displays the smoothly varying pump light intensity and a sharp discontinuity where the intense laser pulse occurred. This spike could be varied in position by adjusting a phase angle dial on the prism turbine. It was found that the maximum output was achieved when the laser was Q-switched 1.9 milliseconds after the pump light began. At any turbine speed the turbine phase angle could be set to give the 1.9 millisecond delay. The Kerr cell laser was already optimized and aligned by the company.

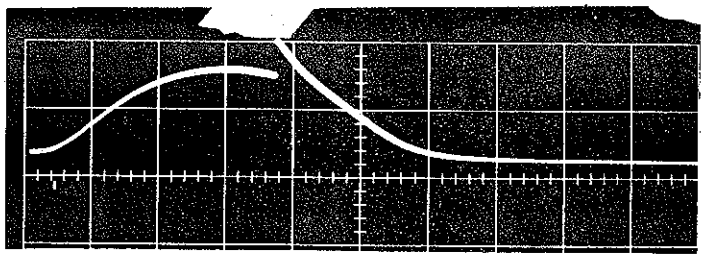

Sweep speed:.5 msec/cm
Amplitude: 5 volts/cm
Turbine speed: 800 rps
Phase angle: 250 deg.

Fig. A-2
Pump Light Monitor Trace

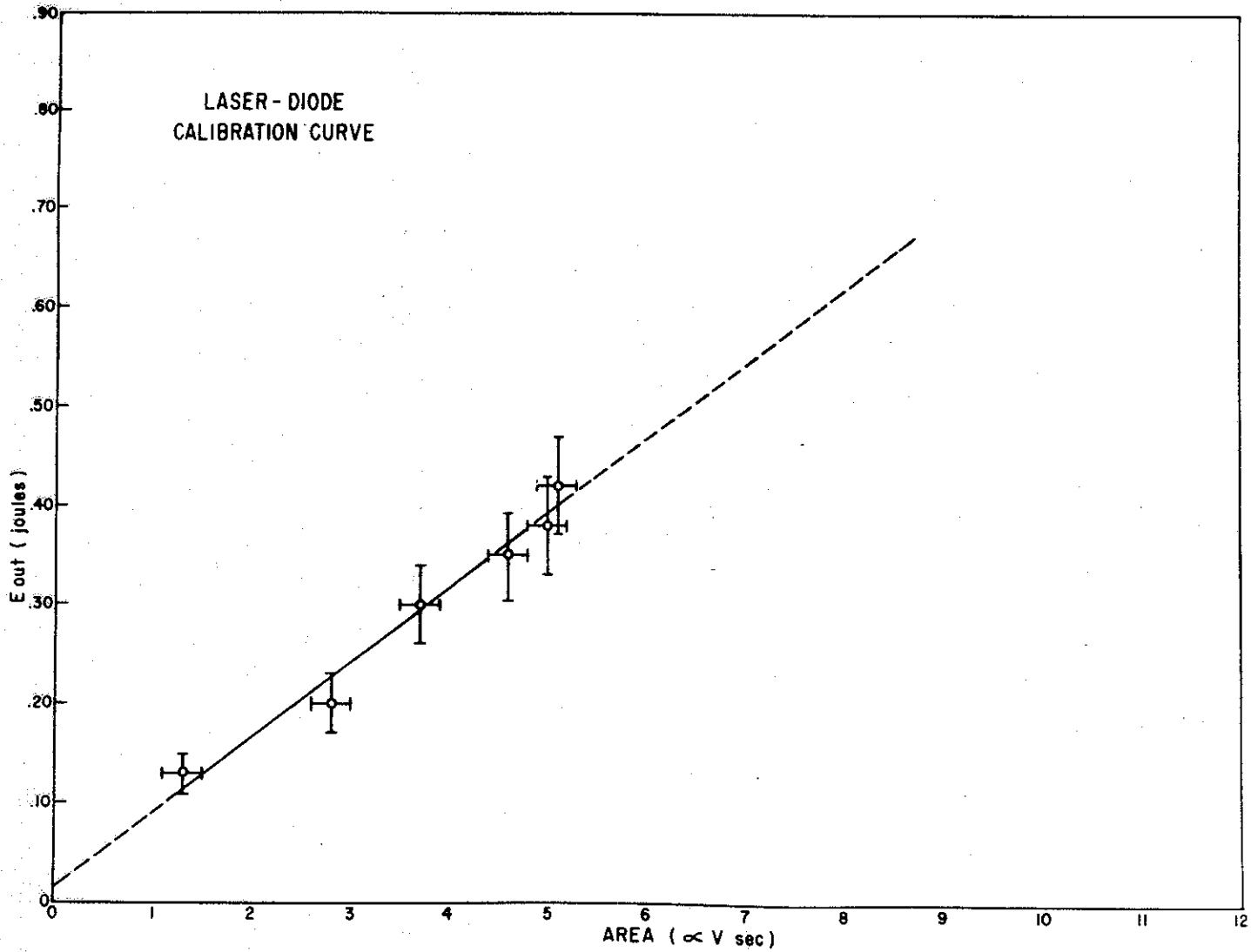

Fig. A-3 Rotating Prism Laser Calibration Curve

Laser Calibration

The energy of each laser shot was determined by correlating the photodiode output signal with some pre-established standard. Prior to the triggering experiments a series of laser shots was taken. The beam was fired into a TRG Laser Rater cone calorimeter and the thermocouple temperature rise indicated on a meter. The device was calibrated by the manufacturer to relate thermocouple current to energy absorbed by the cone. Experience with this instrument has shown it to have an accuracy of ±10%. By varying the pump light input a range of outputs was achieved along with a corresponding amplitude variation of the laser diode signal. For the rotating prism laser the area under the laser diode oscillogram trace was taken as proportional to the energy content. The area was measured with a planimeter and the calibration curve, Fig. A-3, plotted. A straight line fit was made using the least squares technique. The 15% error in energy indicated on each data point is due to the Laser Rater uncertainty and the instrument limit of error for the output meter. The error in area measurement was due to the lack of skill in operating the planimeter. The Kerr cell laser was calibrated by pulse height. Since the pulse widths are all about 10 ns both energy and power are supplied by the same calibration curve. Figure A-4 shows the correlation between oscillogram peak height and Laser Rater energy absorbed. A least square's fit was also made.

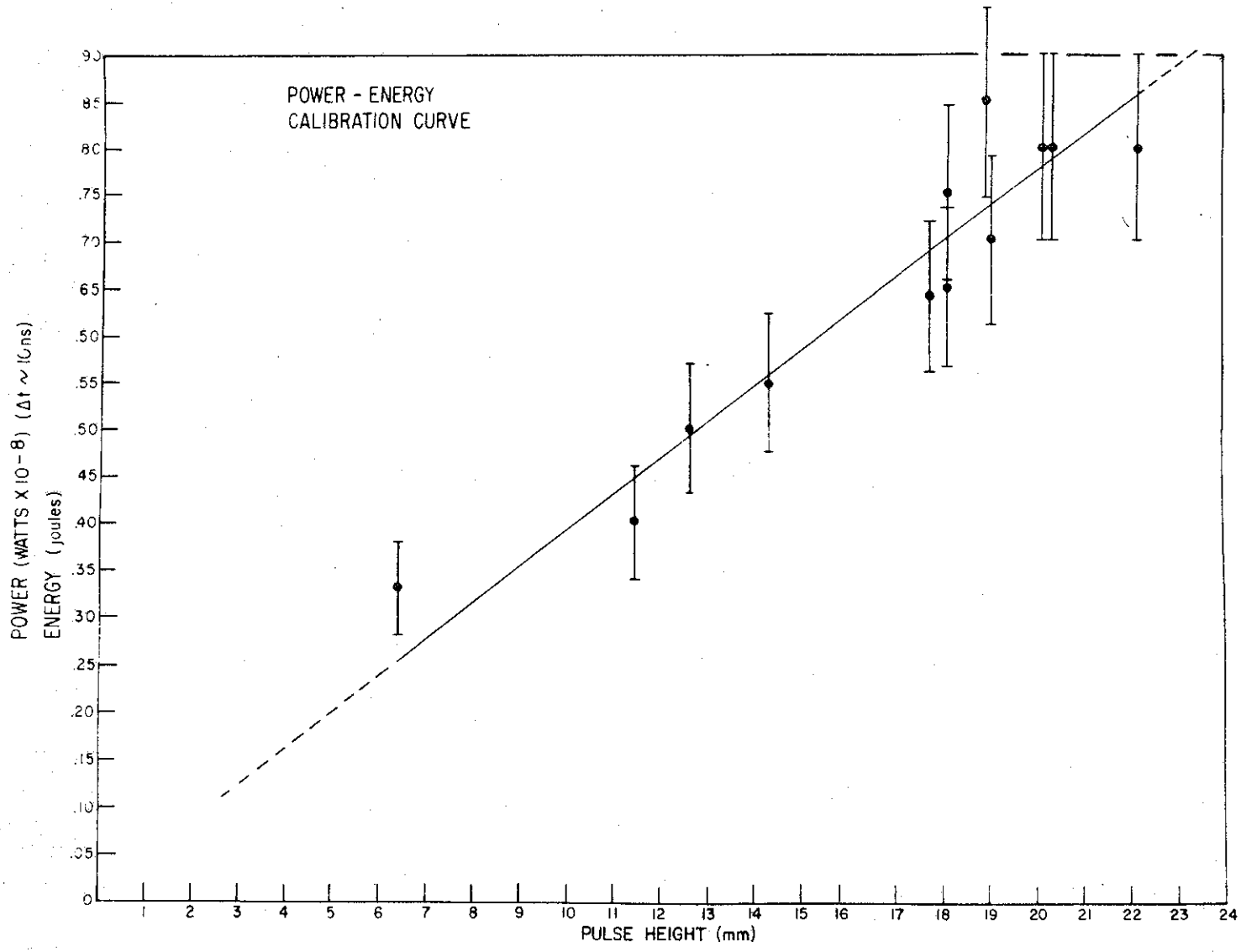

Fig. A-4 Kerr Cell Laser Calibration Curve

Appendix B

Additional Results

This section is included so that the reader may refer to additional data which was obtained. The curves do not substantially deviate from the ones contained in the body of the report.

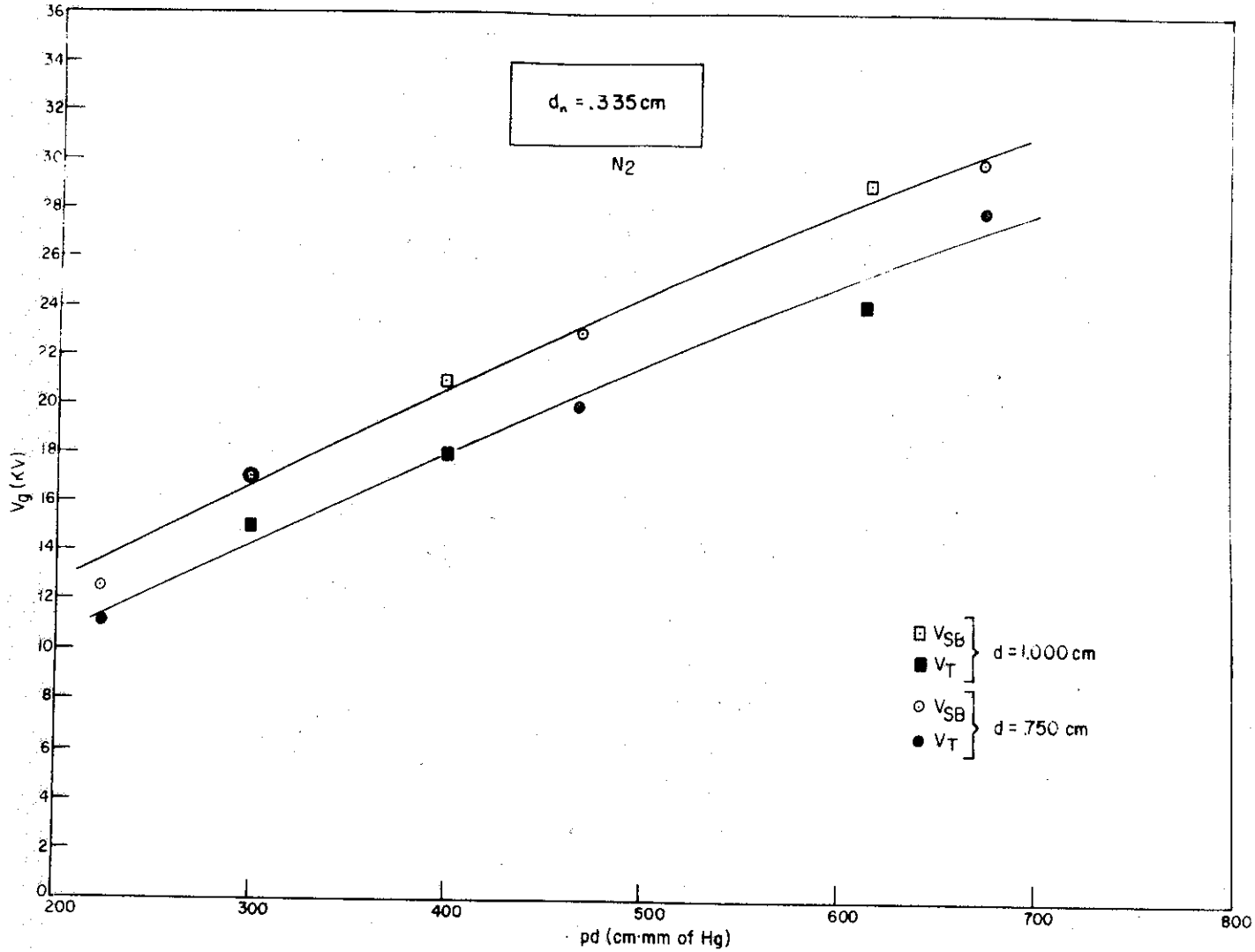

Fig. 8-1 V_{SB} & V_T vs pd (N_2) d_n constant

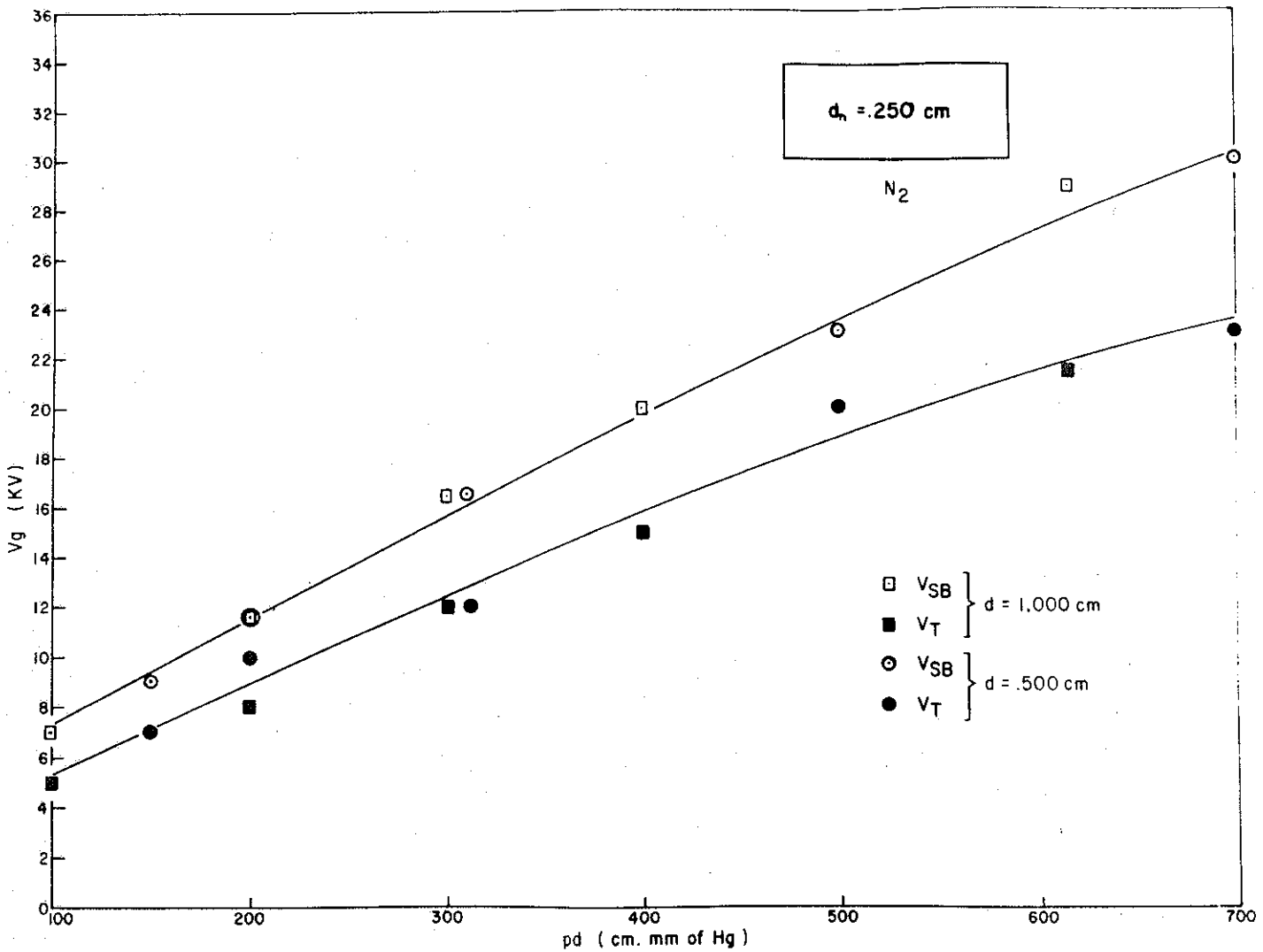

Fig. 3-2 V_{SB} & V_T vs pd (N_2) d_n constant

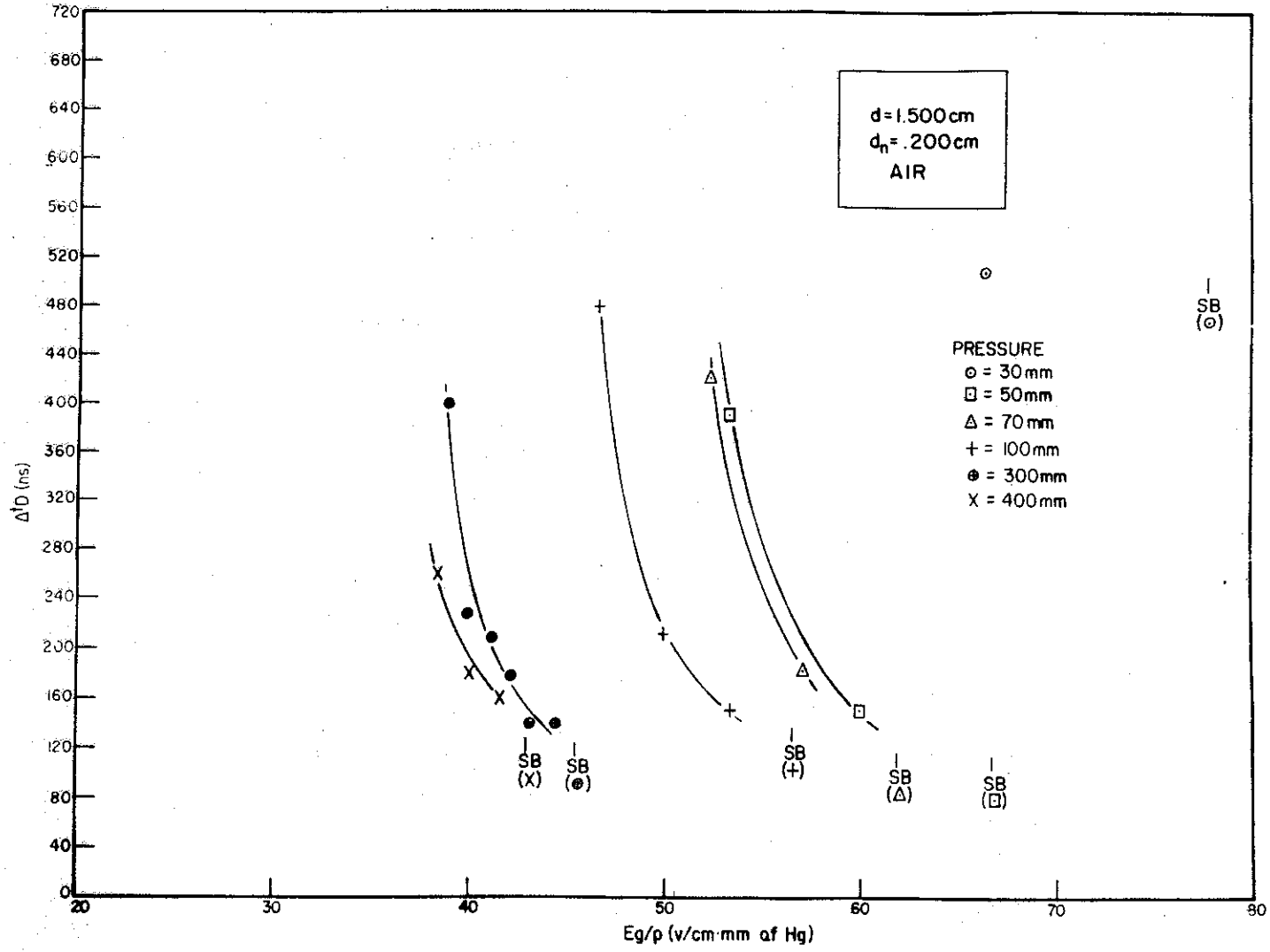

Fig. B-3 Δt_D vs E_g/p (AIR) d, d_n constant

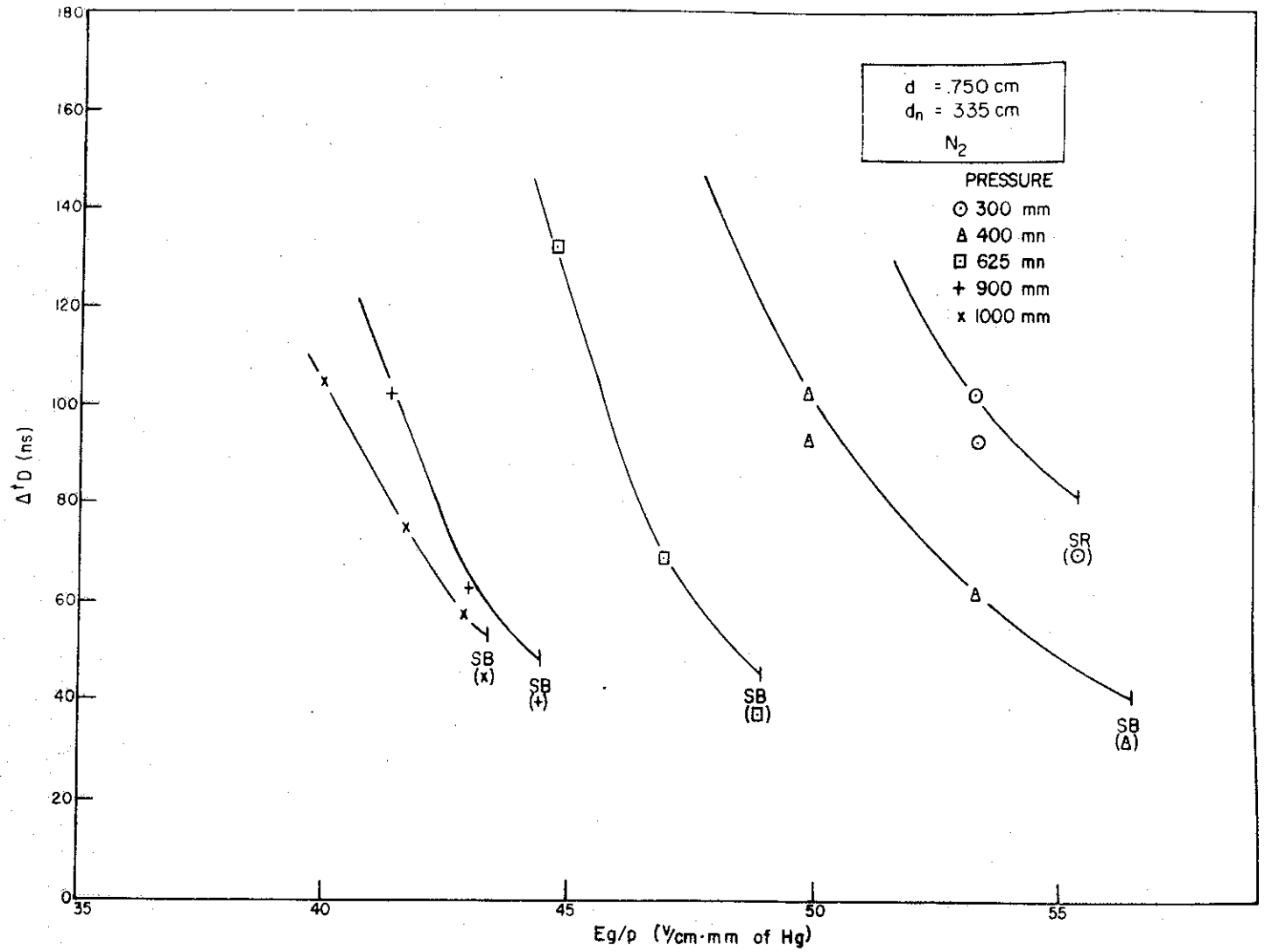

Fig. B-4 Δt_D vs E_g/p (N_2) d, d_n constant

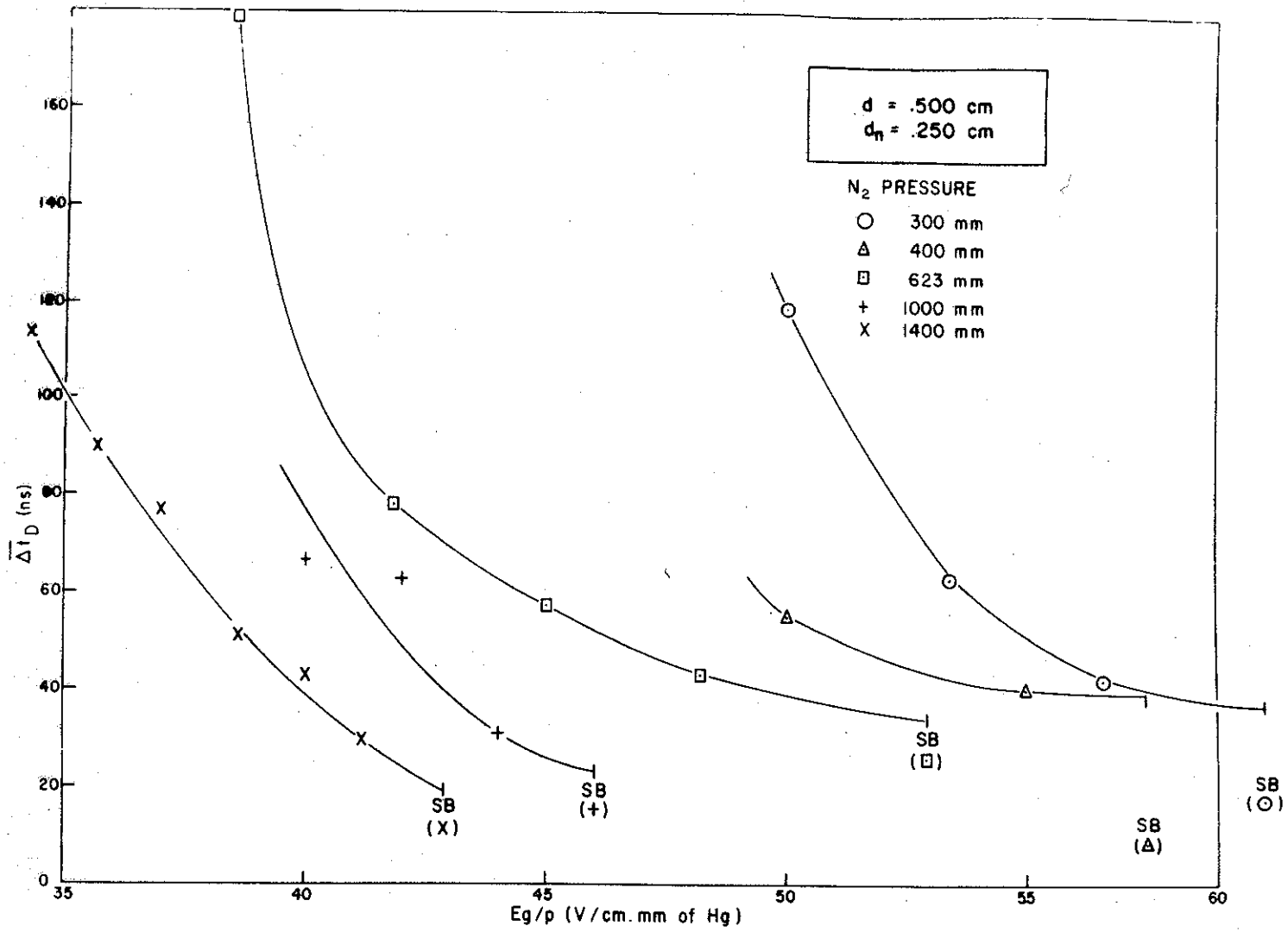

Fig. B-8 $\overline{\Delta t}_D$ vs E_g/p (N_2) d,d_n constant